# Evaluation of SULT1A1-activated alkylators as cytotoxic agents against liver cancer cells

Ke Kong, Wei Zhao, Jonathan H. Shrimp, Marius Vava, Rohan Sinha, Shweta Sharma, Tobie D. Lee, Jacob S. Roth, Olivia W. Lee, Devin Lewis, Sara E. Kearney, Jason M. Rohde, Mindy I. Davis, Pranav Shah, Amy Wang, Xin Xu, Lei Shi,[†] Min Shen, Matthew B. Boxer, Nabeel Bardeesy,[†] Matthew D. Hall, Samarjit Patnaik*

National Center for Advancing Translational Science, National Institute of Health, 9800 Medical Center Drive, Rockville, Maryland 20850

[†]Massachusetts General Hospital Cancer Center, Harvard Medical School, Boston, Massachusetts 02114.

KEYWORDS: Isocitrate dehydrogenase (IDH1), intrahepatic cholangiocarcinoma (ICC), YC-1, sulfotransferase, SULT1A1

ABSTRACT. A quantitative high throughput screen (qHTS) of 7,988 compounds with annotated libraries using biliary tract cancer cell lines with or without isocitrate dehydrogenase I (IDH1) mutations had identified YC-1 as being selectively cytotoxic against the IDH1 mutant cell lines. We present the structure-activity relationship study of YC-1 analogs and identify the key structural motifs that are essential for activity. We highlight the narrow SAR around the furfuryl alcohol that has been reported as a critical motif that is activated by the sulfotransferase enzyme SULT1A1. Drug-like properties of key analogs are evaluated. We also show the SAR of a smaller subset of 2-choloro-4-amino benzyl alcohols from the NCI compound collection with a similar benzyl alcohol motif. We also demonstrate the ability of key analogs to act as substrates of SULT1A1 in a colorimetric biochemical assay.

## Introduction.

Intrahepatic cholangiocarcinoma (ICC) is a rare and aggressive form of biliary tract cancer. Standard of care chemotherapy for patients with unresectable, recurrent, or metastatic biliary tract cancer is systemic treatment with nucleoside analogs such as capecitabine and gemcitabine in combination with platinum complexes such as cisplatin and oxaliplatin (https://www.cancer.gov/types/liver/bile-duct-cancer/). Median survival following diagnosis remains less than a year.[1] The search for dominant molecular alterations that may play a critical role in driving tumorigenesis has revealed that mutations within the isocitrate dehydrogenase genes 1 and 2 (IDH1/2) are often present in ICC that are refractory to chemotherapy. To find synthetic lethal sensitivities present in cells harboring IDH1/2 mutations, we executed a systematic high-throughput screen of approved and experimental therapeutics libraries to identify compounds that selectively kill ICC cell lines harboring IDH1 mutations.[2] To that end, a collection of 7,988 compounds with annotated mechanisms of action and/or pharmacological targets was screened in 8-point dose response against the RBE and SNU-1079 biliary tract cancer cell lines that contain the common R132H and R132C IDH1 mutations, respectively. Counter-screening against biliary tract cell lines CCLP1 and HUCCT1 containing wild type (wt) IDH1 was done to deprioritize cytotoxic compounds towards cells with wt IDH1. A top-ranked compound that emerged from these screening efforts was 3-(5'-hydroxymethyl-2'-furyl)-1-benzyl indazole (YC-1; lificiguat),

which was originally described as an antiplatelet agent (**Figure 1**)[3] and has been proposed to act through a variety of presumably context-specific mechanisms and pathways including soluble guanylyl cyclase activation,[4] hypoxia-inducible factor (HIF)-1α inhibition,[5] and activation of c-Cbl and ERK,[6] among others. However, screening of YC-1 against a broader set of 26 biliary cell lines revealed that YC-1 was also cytotoxic towards cell lines that contain wild type IDH1.[2] This unexpected outcome led to a comprehensive investigation of the mechanism by which YC-1 conferred sensitivity to specific cell lines. Starting with the sensitive RBE cells, incubation with high concentration of YC-1 led to the isolation of six sub-clones that did not respond to YC-1 with no observable cytotoxicity at YC-1 concentrations >25 μM. Proteomics via tandem mass tag (TMT) labeling quantitative mass spectrometry (MS) revealed that the resistant cell lines had significantly reduced expression of the cytosolic sulfotransferase enzyme SULT1A1, a Phase II drug metabolizing enzyme specifically expressed in hepatocytes. In a complementary experiment, knockout of SULT1A1 from the SNU1079 cells (which were sensitive to YC-1) via CRISPR–Cas9 rendered them insensitive to YC-1. This selective SULT1A1-dependent toxicity was tied back to the presence of the furfuryl alcohol in YC-1. A novel mechanism was proposed wherein the alcohol was sulfonated by SULT1A1, and subsequently eliminated to furnish a cationic electrophilic species which was shown via proteomics to selectively alkylate lysines in RNA binding proteins that mediate RNA metabolism, splicing, and translation.[2]

We report here the medicinal chemistry campaign that was carried out on the YC-1 chemical structure to determine the structure-activity relationship (SAR) of its selective cytotoxicity towards RBE and SNU-1079 mIDH1 cells via SULT1A1 activation. All synthesized analogs were also screened against the wt-IDH1-bearing CCLP1 and HUCCT1 cell lines in which there was no appreciable cytotoxicity by YC-1 even at the highest concentrations tested. To drive SAR studies, we evaluated dose-dependent cell-growth inhibition using the CellTiter-Glo™ (Promega) assay. A previously reported biochemical assay that measures SULT1A1 activity was adapted to establish the role key analogs played as enzymatic substrates of SULT1A1. Drug-like properties of select analogs were also examined to determine that the screening hit YC-1 was the best candidate for in vivo evaluation in SULT1A1-dependent tumor models.

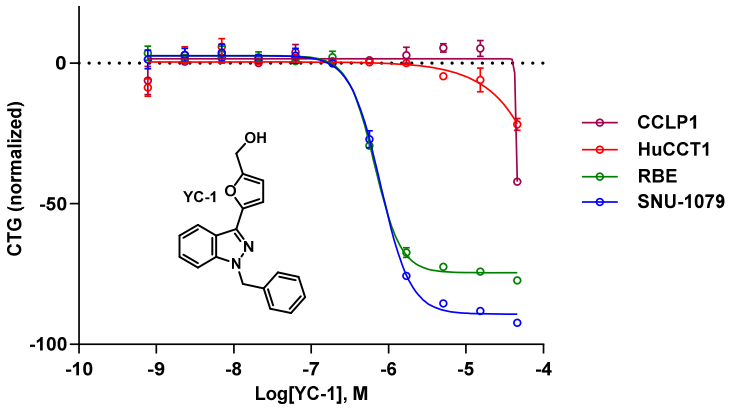


**Figure 1.** Representative $IC_{50}$ curves of in initial HTS hit YC-1 against RBE and SNU-1079 cell lines with mIDH1, and CCLP1 and HUCCT1 cell lines with wt IDH1 (N=3).

**Results and Discussion.**

**Synthesis**. Even though successful routes have previously been disclosed for YC-1 analogs synthesis, most of these routes utilized a Suzuki–Miyaura cross-coupling reaction of the nitrogen-protected 3-iodo indazole core **A** (**Scheme 1**) to attach the northern portion. Thus, to provide a more streamlined access for analog synthesis, we set out to identify an operationally simple procedure that would allow the Suzuki–Miyaura reaction to proceed in the presence of a free indazole N-H. Toward this end, we screened Suzuki coupling conditions between boronic acid **B** and iodide **A** (**Scheme 1**). Due to the thermal instability of the boronic acid, we set the reaction temperature parameter below 45 °C. A quick scan confirmed that none of the reported literature conditions was efficient enough to provide the product with greater than 20% yield. We resorted to implement a Suzuki–Miyaura reaction screen with a KitAlysis™ kit from Sigma Aldrich that contained pre-weighed palladium-based cross-coupling catalysts. This allowed fast screening of 24 different reaction conditions at 1 mmol of substrates and allowed us to identify the combination of APhos-Pd with aq. KOAc as the condition with the highest conversion. These reaction conditions (APhos-Pd, KOAc, DMSO/water, 45 °C) proved to be scalable and generally applicable for an array of substrates. Next the aldehyde product **C** underwent an N-alkylation reaction with various benzylic bromides in the presence of $K_2CO_3$, which was further reduced to provide YC-1 and various analogs in good overall yields. Aldehyde **C** also served as an intermediate in the synthesis of amine-containing analogs. In this case, it was condensed with hydroxylamine and the oxime product was reduced using Zn/AcOH to provide the primary amine in reasonable yield. This streamlined process allowed us to explore SAR in different regions of the molecule with great efficiency.

**Scheme 1**. General scheme of YC-1 analog synthesis.

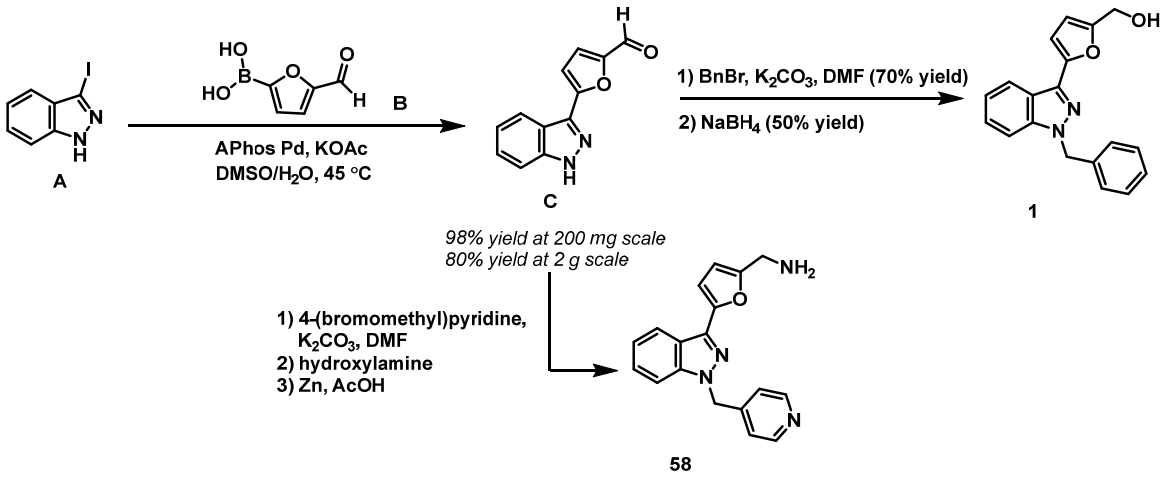


**SAR optimization**. To drive SAR studies, we evaluated dose-dependent cell-growth inhibition using the CellTiter-Glo™ (Promega) and Caspase-Glo™ assays (Promega), and both were found to provide comparable $AC_{50}$'s; this observation was important because YC-1 was found later to induce apoptosis via caspase 3 and caspase 7 activation. Due to the relative operational simplicity, the CellTiter-Glo™ assay was adapted for the SAR campaign. Since the activity of analogs was very similar in both RBE and SNU-1079 cells, for the sake of brevity, activities of all analogs described here will primarily focus on the $IC_{50}$s obtained in RBE cell line. The SAR tables enumerate the capacity of YC-1 analogs to inhibit the viability of sensitive RBE cells with dose dependence by measuring the reduction of ATP concentrations using the CellTiter-Glo™ reagent. $IC_{50}$s are reported only for analogs that show >60% cell-growth inhibition in the concentration

window tested. The percentage reduction of the CellTiter-Glo™ signal at the highest concentration tested (46 μM) is also reported. **Table 1** delineates our focus on the furfuryl alcohol region. We found that the methylene alcohol adjacent to the furan was essential for cellular potency, as one carbon extension to homobenzylic alcohol **2**, capping the alcohol as its methyl ether **3**, or complete removal of the hydroxyl group (**4**) led to dramatic declines in activity. Furthermore, introducing a substituent at the methylene position, such as methyl or cyclopropyl in analogs **5** and **6**, respectively, led to significantly reduced potency. We then took a systematic approach to explore the furan attempting to replace it with more metabolically stable heteroarenes. The potency of these analogs was found to be sensitive to even minor modifications in this region. For instance, introducing an additional nitrogen to the furan, as shown in oxazoles **7**, **8**, and **9**, eroded activity with <50% inhibition even at the highest concentration tested. Similarly, replacing the furan with a thiophene, phenyl, or saturated tetrahydrofuran in compounds **10**, **11**, and **12** was equally detrimental to compounds' activities.

Our SAR trend echoed an earlier report that similarly observed the critical role of the furfuryl alcohol motif to YC-1's HIF-1α inhibitory activities.[7] The exquisite sensitivity of the furfuryl alcohol to minor structural perturbations provided an early indication that this motif might be directly involved in interactions with the target. Next, masking the primary alcohol with an ester group in compound **13** led to a 6-fold decrease in activity compared to parent **1**; this suggested that the alcohol functionality in parent **1** was likely revealed through an esterase-catalyzed hydrolysis of ester **13** in cells. This hypothesis was also supported by compound **14** which had an ester directly attached to the furan and showed a 35% reduction of viability at 46 μM. The corresponding acid **14a** was also tested and found to be inactive. Consistent with the findings that a hydrogen-bond donor at the northern region of the scaffold was necessary for cytotoxic activity, we introduced a primary amine as shown in compound **15**, which proved to be active, albeit 4-fold less potent than YC-1. Amongst all the compounds described in **Table 1**, compound **15** had the most attractive drug-like properties with kinetic solubility >45 μg/mL in aqueous buffer and $t_{1/2}$ >30 min in our high-throughput single-point Rat Liver Microsome (RLM) stability assay. For comparison, YC-1 (**1**) has a solubility of 3 μg/mL and RLM $t_{1/2}$ 6 min in the same assays. Finally, extension of the primary amine to methylamine **16** or hydroxylamine **17** led to >10-fold loss of potency, corroborating our observations of the delicate nature of the SAR.

We then turned our attention to the N-benzyl moiety in the southern region of YC-1 (**Table 2**). Removing the N-substituent entirely (compound **18**) or replacing with a small aliphatic group such as methyl (compound **19**) or isoprenyl (**20**) led to partial inhibition. Completely removing the spacer (**22**) or increasing the spacer length to two carbons (**23**) led to reduced potency, indicating the preference of a one-carbon spacer in the benzyl group of YC-1. Similarly, the nature of the spacer appeared to be important as replacing the methylene linker with a carbonyl (**24**), sulfone (**25**), or carbamate (**26**) resulted in inferior activity. A small hydrophobic methyl group added to the methylene spacer (**27**) registered an $IC_{50}$ of ~4 μM. The SAR in Table 2 emphasized that the optimal spacer in the southern region was the one-carbon methylene group seen in YC-1.

**Table 1.** SAR of the northern furfuryl alcohol.

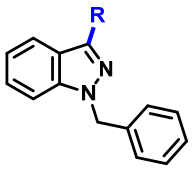


| compound | R | $IC_{50}$[a] (μM) | % Resp[b] @46 μM |
|---|---|---|---|
| **1.** | 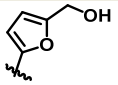 | 0.66 | -75 |
| **2.** | 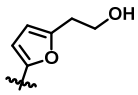 | ND | -21 |
| **3.** | 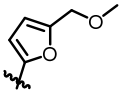 | ND | -49 |
| **4.** |  | ND | -59 |
| **5.** | 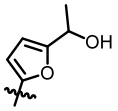 | ND | -64 |
| **6.** | 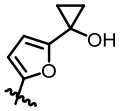 | ND | -42 |
| **7.** | 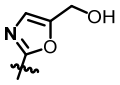 | ND | -16 |
| **8.** | 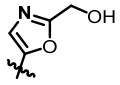 | ND | -21 |
| **9.** | 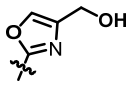 | ND | -32 |

| compound | R | $IC_{50}$[a] (μM) | % Resp[b] @46 μM |
|---|---|---|---|
| **10.** | 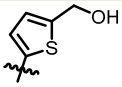 | ND | -30 |
| **11.** | 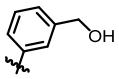 | ND | -28 |
| **12.** | 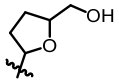 | ND | -13 |
| **13.** | 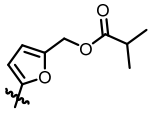 | 4.15 | -62 |
| **14.** | 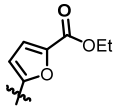 | ND | -35 |
| **14a.** | 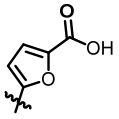 | ND | 0 |
| **15.** | 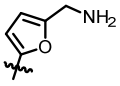 | 2.34 | -70 |
| **16.** | 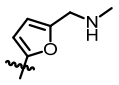 | 20.82 | -84 |
| **17.** | 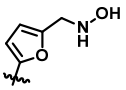 | ND | -52 |

[a]$IC_{50}$s are reported as an average of N=3 from a 11-pt dose response CellTiter-Glo™ assay in RBE cells. $IC_{50}$s and are not determined (ND) when response in cell viability is <60% of DMSO control at the maximum compound concentration of 46 μM tested in the assay. [b]This is the % response compared to DMSO control in the CellTiter-Glo™ assay at the highest concentration (46 μM) tested.

**Table 2**. SAR of the southern region linker.

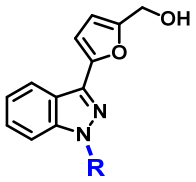


| compound | R | $IC_{50}$[a] (μM) | % Resp[b] @46 μM |
|---|---|---|---|
| **18.** |  | ND | -62 |
| **19.** |  | ND | -56 |
| **20.** |  | ND | -48 |
| **21.** | 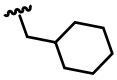 | 16.53 | -82 |
| **22.** |  | 4.15 | -78 |

| compound | R | $IC_{50}$[a] (μM) | % Resp[b] @46 μM |
|---|---|---|---|
| **23.** | 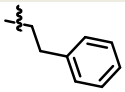 | 5.87 | -73 |
| **24.** | 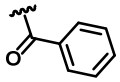 | ND | -58 |
| **25.** | 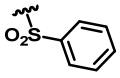 | ND | -6 |
| **26.** | 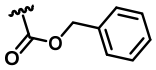 | ND | -55 |
| **27.** | 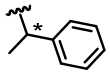 | 4.15 | -76 |

[a]$IC_{50}$s are reported as an average of N=3 from a 11-pt dose response CellTiter-Glo™ assay in RBE cells. $IC_{50}$s and are not determined (ND) when response in cell viability is <60% of DMSO control at the maximum compound concentration of 46 μM tested in the assay. [b]This is the % response compared to DMSO control in the CellTiter-Glo™ assay at the highest concentration (46 μM) tested.

Retaining the optimal one-carbon spacer, we embarked on the SAR exploration of the southern phenyl ring itself (**Table 3**). The addition of small substituents including fluorine (compounds **28-30**), chlorine (compounds **31-33**), methyl (compounds **34-36**), and methoxy groups (**37-39**) at the ortho, meta, or para positions of the phenyl ring was tolerated. Notably the ortho- and meta-OMe groups in analogs **37** and **38** offered slightly better potencies than YC-1. Similarly, introducing 2-pyridine (**40**), 3-pyridine (**41**), or 4-pyridine (**42**) in place of the benzyl group also led to improved potencies. However, incorporating more heteroatoms as in pyrimidine **43** and thiazole **44** failed to bring additional benefits. Combining the two beneficial elements, a ring nitrogen and a methoxy substituent, provided compounds **45-47** with analog **45** registering a benchmark $IC_{50}$ of 0.21 μM. Finally, the relative flexibility of the southern region binding domain allowed introducing a polyethyleneglycol-linked biotin to analog **48** without significantly sacrificing the selectivity, a tool compound that proved to be valuable in supporting our reported efforts in elucidating YC-1's mechanism of action.[2]

The SAR of the indazole core structure was also investigated. For ease of comparison, alternate cores with a benzyl group and furfuryl alcohol in the southern and northern regions, respectively, as embedded in YC-1, were prepared (**Table 4**). Walking a nitrogen atom from the 4- to the 7-position (compounds **49-52**) showed very interesting SAR with analog **49** featuring the nitrogen

at the 4-position being the only tolerated iteration. The introduction of nitrogen in compounds **49-52** improved the aqueous solubility in our kinetic solubility assay to >45 μg/mL compared to YC-1's solubility of 3 μg/mL in the same assay. The introduction of a halogen such as the 4-Cl derivative **53** showed a reduction of activity whereas a smaller 5-F in analog **54** maintained potency. Changing the core to indole **55** led to a 10-fold drop in potency compared to YC-1. Fusing a cyclohexyl ring to the indazole (**56**) caused a smaller two-fold potency decrease. The pyrazole core **57** was also synthesized and proved to be much weaker.

To improve the drug-like properties of the YC-1 scaffold, we synthesized a final set of analogs as illustrated in **Table 5**. We incorporated the 4-nitrogen in the indazole core and an additional nitrogen in the southern benzyl ring in analogs **60-63**: these compounds had aqueous solubilities of >30 μg/mL and $t_{1/2}$ >15 min in rat, mouse, and human liver microsomes (LM). Unfortunately, their primary RBE cytotoxic activity was dampened compared to YC-1. At this point, our mechanistic studies had provided evidence that the northern hydroxyl group, upon in-situ sulfonation by SULT1A1 and elimination, acted as an electrophilic alkylator to lysines on the surface of RNA binding proteins in cancer cells. (**Figure 2**).[2] Thus, we were interested in exploring the additional possibility that a primary amine in this region could also function similarly as an alkylator. Encouraged by the activity of furfuryl amine **15** (RBE $IC_{50}$ 2.34 μM) in Table 1, we prepared analogs **58**, **59,** and **63**. In this set only compound **58**, which was prepared by combining the southern 4-pyridyl group with the primary amine in the northern region, retained its potency. It also had improved microsome stability (rat, mouse, human LM $t_{1/2}$ ~17, 37, 777 min, respectively) and aqueous solubility >30 μg/mL.

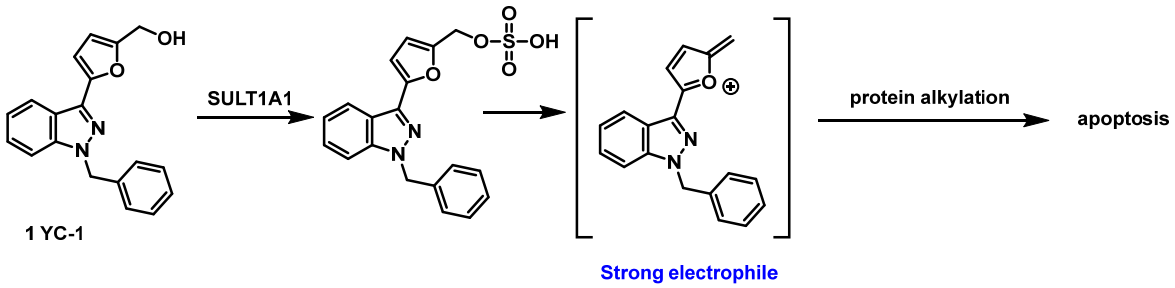


**Figure 2**. Proposed mechanism of SULT1A1-mediated bioactivation of YC-1.

**Table 6** enumerates the cytotoxic activity of key analogs from our SAR campaign against the four biliary tract cancer cell lines that were used in the screening. As expected, the activity was very similar in the RBE and SNU-1079 cells with mIDH1 with almost complete inactivity against the HuCCT1 and CCLP1 with wt IDH1. The rat liver microsome (RLM) stability was the best for compound **15** and analog **58** was second with RLM $t_{1/2}$ of 17 min. The passive permeability as determined by PAMPA was high for the chemical series; there were also multiple compounds with improved solubility (**Table 6**). Based on this data, compounds **15** and **58** were advanced to mouse pharmacokinetics.

**Table 3.** Modification of the southern phenyl moiety

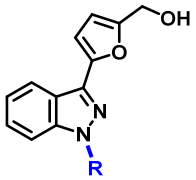


| compound | R | $IC_{50}$[a] (μM) | % Resp[b] @46 μM |
|---|---|---|---|
| **28.** | 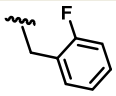 | 1.17 | -68 |
| **29.** | 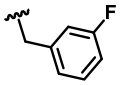 | 1.17 | -60 |
| **30.** | 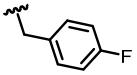 | 1.31 | -66 |
| **31.** | 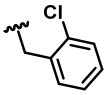 | 1.47 | -63 |
| **32.** | 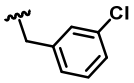 | 1.47 | -75 |
| **33.** | 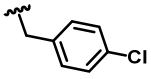 | 1.65 | -70 |
| **34.** | 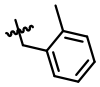 | 1.31 | -61 |
| **35.** | 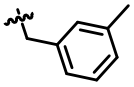 | 2.62 | -73 |
| **36.** | 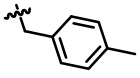 | 1.65 | -59 |
| **37.** | 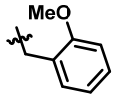 | 0.47 | -74 |
| **38.** | 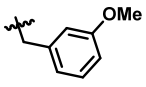 | 0.47 | -76 |

| compound | R | $IC_{50}$[a] (μM) | % Resp[b] @46 μM |
|---|---|---|---|
| **39.** | 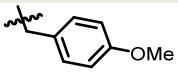 | 1.17 | -70 |
| **40.** | 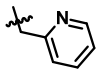 | 0.29 | -70 |
| **41.** | 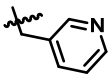 | 0.26 | -75 |
| **42.** | 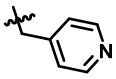 | 0.17 | -57 |
| **43.** | 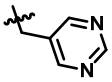 | 1.04 | -71 |
| **44.** | 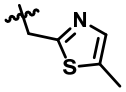 | 1.04 | -81 |
| **45.** | 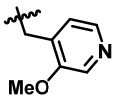 | 0.21 | -85 |
| **46.** | 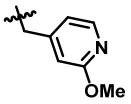 | 0.37 | -62 |
| **47.** | 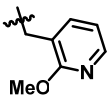 | 0.23 | -50 |
| **48.** | 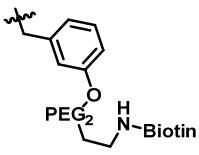 | 4.66 | -66 |

[a]$IC_{50}$s are reported as an average of N=3 from a 11-pt dose response CellTiter-Glo™ assay in RBE cells. $IC_{50}$s and are not determined (ND) when response in cell viability is <60% of DMSO control at the maximum compound concentration of 46 μM

tested in the assay. [b]This is the % response compared to DMSO control in the CellTiter-Glo™ assay at the highest concentration (46 μM) tested

**Table 4.** Core modifications

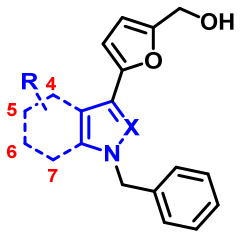


| compound | R | $IC_{50}$[a] (μM) | % Resp[b] @46 μM |
|---|---|---|---|
| **49.** | 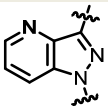 | 2.34 | -65 |
| **50.** | 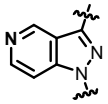 | ND | -47 |
| **51.** | 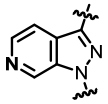 | ND | -17 |
| **52.** | 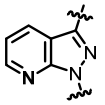 | 14.74 | -51 |
| **53.** | 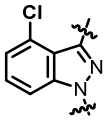 | 5.87 | -86 |
| **54.** | 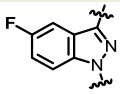 | 0.93 | -72 |
| **55.** | 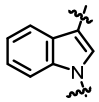 | 7.39 | -85 |
| **56.** | 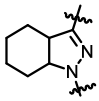 | 1.47 | -62 |
| **57.** | 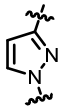 | ND | -47 |

[a]$IC_{50}$s are reported as an average of N=3 from a 11-pt dose response CellTiter-Glo™ assay in RBE cells. $IC_{50}$s and are not determined (ND) when response in cell viability is <60% of DMSO control at the maximum compound concentration of 46 μM tested in the assay. [b]This is the % response compared to DMSO control in the CellTiter-Glo™ assay at the highest concentration (46 μM) tested

**Table 5**. Combinations of modifications

| compound | Structure | $IC_{50}$[a] (μM) | % Resp[b] @46 μM |
|---|---|---|---|
| **58.** | 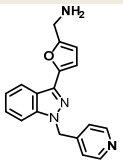 | 0.59 | -68 |
| **59.** | 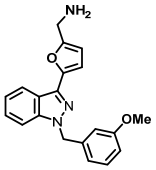 | 5.23 | -78 |
| **60.** | 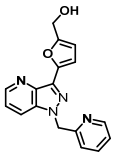 | 2.34 | -76 |
| **61.** | 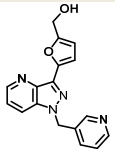 | 5.23 | -80 |
| **62.** | 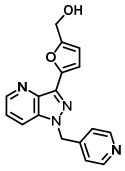 | 8.29 | -73 |
| **63.** | 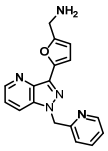 | 2.94 | -74 |

[a]$IC_{50}$s are reported as an average of N=3 from a 11-pt dose response CellTiter-Glo™ assay in RBE cells. $IC_{50}$s and are not determined (ND) when response in cell viability is <60% of DMSO control at the maximum compound concentration of 46 μM tested in the assay. [b]This is the % response compared to DMSO control in the CellTiter-Glo™ assay at the highest concentration (46 μM) tested

**Table 6**. In vitro drug like parameters of representative analogs

| Cpd# | RBE $IC_{50}$ μM | SNU-1079 $IC_{50}$ μM | HuCCT1 $IC_{50}$ μM | CCLP1 $IC_{50}$ μM | RLM $t_{1/2}$ [a] min | PAMPA pH 7.4 $10^{-6}$ cm/s | Solubility μg/mL |
|---|---|---|---|---|---|---|---|
| **1** | 0.66 | 0.830 | >46 | >46 | 6 | 842 | 3 |
| **15** | 2.34 | 2.620 | >46 | >46 | >30 | ND | >45 |
| **37** | 0.47 | 0.410 | >46 | ~46 | 2 | 180 | 1 |
| **38** | 0.47 | 0.47 | >46 | >46 | 2 | 1374 | 1 |
| **40** | 0.29 | 0.420 | >46 | >46 | 11 | 425 | >45 |
| **41** | 0.26 | 0.370 | >46 | ~46 | 11 | 250 | >45 |
| **42** | 0.17 | 0.230 | >46 | >46 | 12 | 518 | >45 |
| **45** | 0.21 | 0.170 | >46 | >46 | 7 | 765 | >33 |
| **46** | 0.37 | 0.410 | >46 | >46 | 7 | 1336 | >33 |
| **47** | 0.23 | 0.210 | >46 | >46 | 6 | 1186 | >33 |
| **58** | 0.59 | 0.470 | >46 | >46 | 17[b] | 1294 | >30 |

ND Not Determined. [a]$t_{1/2}$ is determined as an extrapolation of % parent remaining after 15 minute incubation with RLM. [b]This RLM $t_{1/2}$ was determined in a multi-point experiment.

**Pharmacokinetics (PK)**. Compounds **15**, **58,** and YC-1 (**1**) were evaluated in mouse PK experiments to help select a candidate for efficacy experiments. The plasma exposure for each compound was evaluated in male CD1 mice after dosing via intravenous (IV), oral (PO), and intraperitoneal (IP) routes at 5, 10, 30 $mgkg^{-1}$. **Table 7** showcases PK parameters calculated. Highest plasma concentrations, $C_0$ in the IV and $C_{max}$ in the IP and PO, were achieved with YC-1 **1** in every experiment. Among the three routes of administration, oral route had the lowest AUCs for all three compounds, while the intraperitoneal route offered best exposures with analog **58** having the highest AUC in this set. The in vivo clearance, as determined in the IV dosing experiments, seemed high and similar for all three compounds. This was disappointing as the in vitro microsomal stability, especially for compound **58**, was high. We speculate that high clearance could be due to Phase II metabolizing enzymes acting directly on the free alcohol or amine present in these molecules leading to the elimination of the parent from the blood. This rationale is in line with the mechanism by which YC-1 transforms into an alkylator via sulfonation by SULT1A1 which is a Phase II metabolizing enzyme itself. The plasma concentration versus time profiles are plotted in **Figure 3** for compounds **1** and **58**; both compounds reach peak concentrations in <1 hr and analog **58** is cleared at a slower rate compared to YC-1.

**Table 7.** Pharmacokinetics parameters of key compounds

| Cpd # | Route | Dose (mg/kg) | $CL_{obs}$ (mL/min/kg) | $t_{1/2}$ (h) | $t_{max}$ (h) | $C_0$ (ng/mL) | $C_{max}$ (ng/mL) | $AUC_{last}$ (h*ng/mL) | $AUC_{last}$/Dose (h*mg/mL) | $V_{ss}$_obs (L/kg) | F (%) |
|---|---|---|---|---|---|---|---|---|---|---|---|
| **1** | IV | 5 | 77.9 | 1.39 | | 5095 | | 1066 | 213 | 2.68 | |
| | PO | 10 | | 1.86 | 0.25 | | 220 | 218 | 22 | | 11 |
| | IP | 30 | | 1.3 | 0.25 | | 5537 | 3367 | 112 | | 52 |
| **15** | IV | 5 | 78.9 | 5.4 | | 1360 | | 1054 | 211 | 17.34 | |
| | PO | 10 | | 1.75 | 0.5 | | 168 | 314 | 31 | | 15 |
| | IP | 30 | | 5.69 | 0.33 | | 1147 | 5240 | 175 | | 84 |
| **58** | IV | 5 | 67.1 | 1.08 | | 1515 | | 1313 | 263 | 4.01 | |
| | PO | 10 | | 1.74 | 0.5 | | 395 | 891 | 89 | | 34 |
| | IP | 30 | | 2.33 | 0.5 | | 4033 | 9118 | 304 | | 116 |

**Figure 3**. Plasma conc. vs. time plots for YC-1 and compound **58** in male CD1 mice.

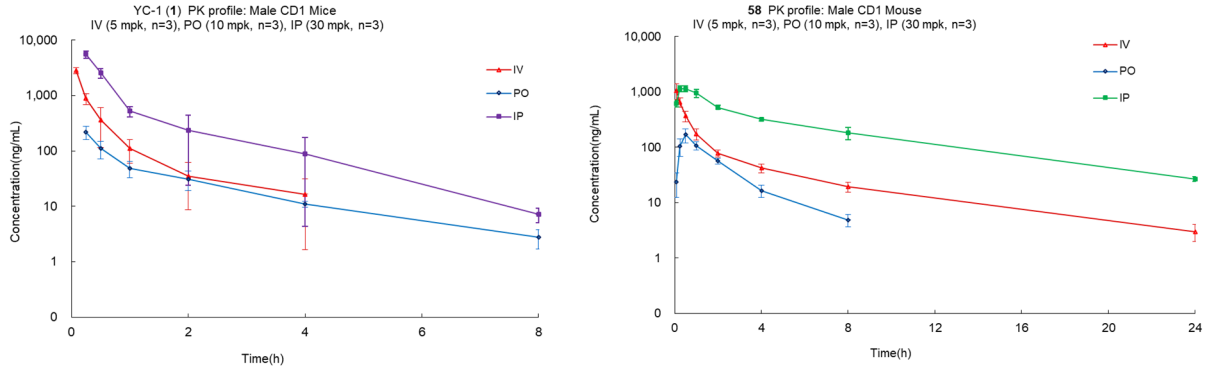

**YC-1** (**1**) was dosed as solution in PEG300/30% solutol in water/ Saline (30/17/54) and **58** was dosed as solution in 5% NMP, 20% PEG 300 and 75% of a solutol HS 15 in water (15 wt%). 24-hr time point concentration for YC-1 was below LLQ (Lower limit of quantification).

**Warhead exploration.** Though the medicinal chemistry campaign had utilized cytotoxicity against cell lines with mIDH1 to drive structure- activity relationship studies, we had discovered that this activity was strongly correlated to the expression of SULT1A1.[2] Our SAR studies suggested that the furfuryl alcohol was the key element for activity. To that end, we decided to examine if compounds with similar motifs could elicit cytotoxicity via SULT1A1-mediated sulfonation as proposed in **Figure 2**. We approached this analysis by investigating the annotated cytotoxicity profiles of >22,000 compounds in the NCI60[8] and used the CellMiner NCI-60 tool to identify molecules whose cytotoxicity positively correlated with SULT1A1 expression across the sixty cell lines.[9] We have reported the findings of our analysis, by which we found within the top 150 compounds, candidates whose activities have been linked to SULT1A1; these included analogs of oncrasin-1 (N-benzyl indole carbinol (N-BIC), RITA (reactivating p53 and inducing tumor apoptosis, compound **104** in **Table 9**) and amino flavones.[10-13] Another group of compounds that was very well represented in this set was a series of 88 amino halogenated benzyl alcohols (AHBA). We obtained representative compounds from the NCI compound collection library and tested them for cytotoxicity against the same cell lines we used to drive the SAR studies around YC1; **Tables 8 and 9** shows a snapshot of the SAR in RBE cells where most compounds belong to a 2-choloro 4-amino benzyl alcohol series. With a constant 4-N-ethyl group, we found a variety of substitutions were tolerated in the phenyl ring attached to the N-benzyl substituent (**Table 8**). Analogs **65-75** showcase a systematic evaluation of a single F, Cl, Me and OMe substitution and analogs **76-83** show the effects of double substitutions. Several compounds in this set (highlighted in green) had $IC_{50}$s <200 nM and >75% activity at the top 46 μM concentration tested. Replacing this phenyl ring with a pyridine ring led to >2-fold loss on the potencies compared to parent **64**. Then we looked at some compounds where we maintained a 4-fluorobenzyl nitrogen substitution and scanned alkyl groups at the 4-amine (**Table 9**). Smaller substitutions linked with a methylene were tolerated (analogs **87-89**), but immediate branching (cyclobutyl **90**) and a larger benzyl group (**91**) were less active. Cyclization of the benzyl amine to tetrahydroisoquinolines **92-94** was possible and produced analogs **92** and **93** with <200 nM $IC_{50}$. The activity of the known di-thiophenyl alcohol RITA **95** is also shown in **Table 9**.[14, 15]

**Table 8** SAR of 2-chloro-4-aminobenzyl alcohol series

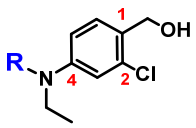


| cmpd | R | | $IC_{50}$[a] (μM) | % Resp[b] @46 μM |
|---|---|---|---|---|
| 64 | 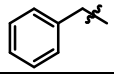 | | 0.12 | -57 |
| 65 | 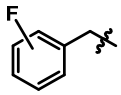 | *o*-F | 0.29 | -61 |
| 66 | | *m*-F | 0.17 | -54 |
| 67 | | *p*-F | 0.17 | -53 |
| 68 | 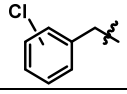 | *o*-Cl | 0.23 | -87 |
| 69 | | *m*-Cl | 0.23 | -59 |
| 70 | 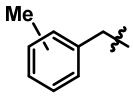 | *o*-Me | 0.52 | -87 |
| 71 | | *m*-Me | 0.23 | -85 |
| 72 | | *p*-Me | 0.37 | -95 |
| 73 | 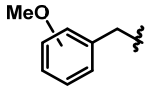 | *o*-OMe | 0.42 | -66 |
| 74 | | *m*-OMe | 0.12 | -82 |
| 75 | | *p*-OMe | 0.21 | -83 |
| 76 | | *o,m*-diF | 0.13 | -56 |
| 77 | | *o,p*-diF | 0.21 | -82 |
| 78 | | *o,o'*-diF | 0.07 | -57 |
| 79 | 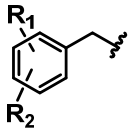 | *m,m'*-diF | 0.12 | -81 |
| 80 | | *o,o'*-F, Cl | 0.15 | -54 |
| 81 | | *o,o'*-F, OMe | 0.15 | -65 |
| 82 | | *o,o'*-F, $CF_3$ | 0.15 | -57 |
| 83 | | *o,o'*-diCl | 0.15 | -59 |
| 84 | 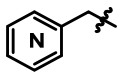 | *o*-N | 0.42 | -52 |
| 85 | | *m*-N | 0.37 | -54 |
| 86 | | *p*-N | 0.93 | -83 |

**Table 9**. SAR of 2-chloro-4-aminobenzyl alcohol series

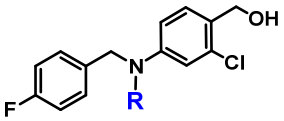


| cmpd | R | $IC_{50}$[a] (μM) | % Resp[b] @46 μM |
|---|---|---|---|
| 87. |  | 0.26 | -89 |
| 88. | 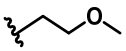 | 0.37 | -75 |
| 89. | 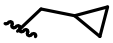 | 0.26 | -55 |
| 90. |  | 0.74 | -84 |
| 91. | 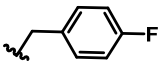 | 2.6 | -78 |

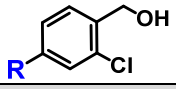


| | R | $IC_{50}$[a] (μM) | % Resp[b] @46 μM |
|---|---|---|---|
| 92. | 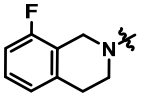 | 0.17 | -87 |
| 93. | 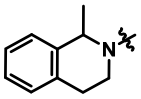 | 0.19 | -91 |
| 94. | 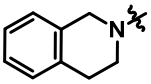 | 0.23 | -84 |

| | RITA | $IC_{50}$[a] (μM) | % Resp[b] @46 μM |
|---|---|---|---|
| 95. | 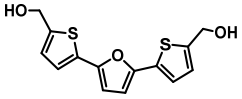 | 0.12 | -60.3 |

$IC_{50}$s are reported as an average of N=3 from a 11-pt dose response CellTiter-Glo™ assay in RBE cells and are not determined (ND) when response in cell viability is <50% of DMSO control at the maximum compound concentration of 46 μM tested in the assay

**SULT1A1 activity**. To directly characterize the ability of compounds to serve as SULT1A1 substrates, we established a biochemical colorimetric assay that utilized E. coli-derived human SULT1A1 protein. The assay utilizes the canonical cofactor 3'-phosphoadenosine-5'-phosphosulfate (PAPS) as the sulfate donor which is converted to the byproduct 3'-phosphoadenosine-5'-phosphate (PAP). PAP can be quantitated by its conversion back to PAPS by SULT1A1 using p-nitrophenyl sulfate. This biochemical reaction produces p-nitrophenolate that can be quantified by measuring absorbance at 405 nm.

We first evaluated the kinetics of YC-1 sulfonation at multiple concentrations by following the p-nitrophenolate signal over 145 min (**Figure 4A**). We observed concentration-dependent increase in signal and signal saturation at the highest doses of 30 and 100 μM kinetics after ~75 and 90 min respectively.

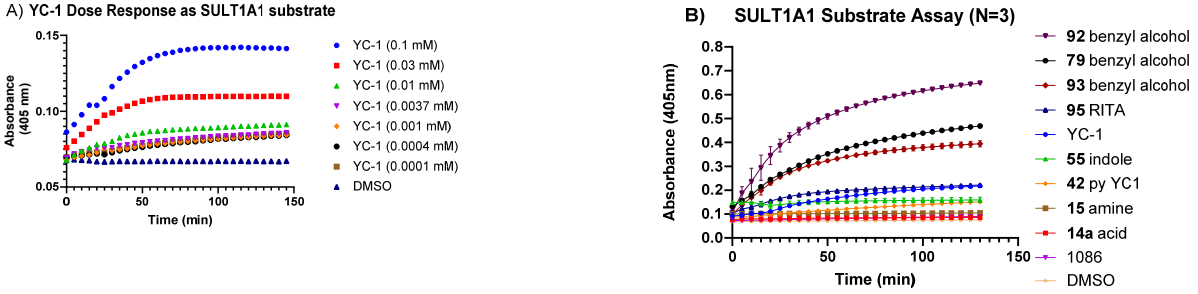


**Figure 4**. **A**) Absorbance at 405 nm from *p*-nitrophenolate was measured while various concentrations of YC-1 were added to SULT1A1 in the biochemical colorimetric assay. **B**) Absorbance at 405 nm from p-nitrophenolate was measured as 100 μM of each small molecule was added to SULT1A1 in the biochemical colorimetric assay.

Since the throughput of the assay was relatively low, we selected 10 analogs from our SAR exploration with a spectrum of cytotoxic activities and distinct chemical structures to be characterized as SULT1A1 substrates. **Figure 4B** compares the conversion of these compounds kinetically in the same plot at 100 μM, and **Figure 5** reports the activity at the assay endpoint (120 min) in a histogram. The benzyl alcohols **79**, **92**, and **93** appeared to be the strongest substrates in this biochemical assay; these compounds had the best correlation between their cytotoxicity and substrate activity in the SULT1A1 biochemical assay. They are followed by RITA **95**, YC-1, and the YC-1 pyridine analog **42**; these were quite potent in the RBE assay, but they showed <2-fold response in the SULT1A1 assay compared to the benzyl alcohols.

Compounds in which the alcohol of the YC-1 parent structure was replaced within an amine (**15**, **58**) proved to be poor substrates, despite their cytotoxicity. This implies that these benzylic amines may not serve as substrates for SULT1A1, and their cytotoxicity may be mediated via other mechanisms. However, metabolism identification studies demonstrated that we had also selected inactive acid **14a** and indole **55** with intermediate cytotoxicity activity; both analogs had negligible signals. RITA (**95**) whose activity has been shown to depend on high SULT1A1 expression was the positive control in the assay and exhibited substrate turnover supporting the physiological basis of the colorimetric biochemical assay.[16]

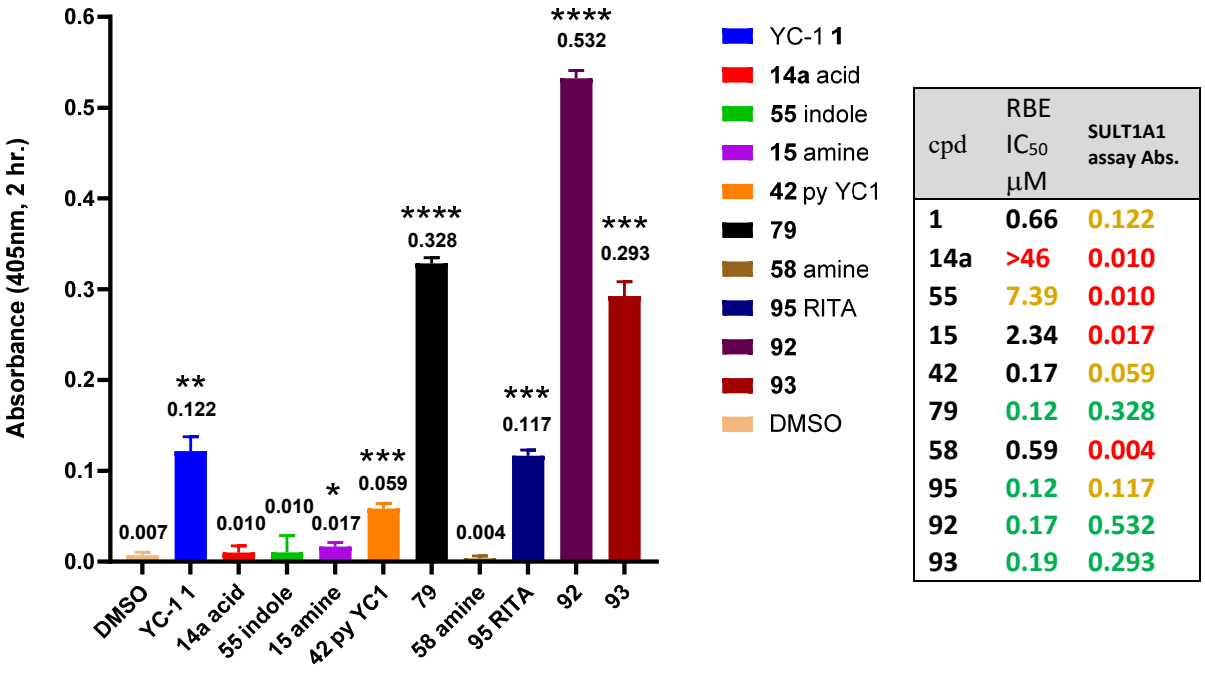


| cpd | RBE $IC_{50}$ μM | SULT1A1 assay Abs. |
|---|---|---|
| 1 | 0.66 | 0.122 |
| 14a | >46 | 0.010 |
| 55 | 7.39 | 0.010 |
| 15 | 2.34 | 0.017 |
| 42 | 0.17 | 0.059 |
| 79 | 0.12 | 0.328 |
| 58 | 0.59 | 0.004 |
| 95 | 0.12 | 0.117 |
| 92 | 0.17 | 0.532 |
| 93 | 0.19 | 0.293 |

**Figure 5. Evaluating YC-1 and analogs as SULT1A1 substrates**. Quantified absorbance from the colorimetric SULT1A1 activity assay at two hours to identify substrates of SULT1A1 sulfonation at 100 μM concentration. *$p \leq 0.05$ vs DMSO; **$p \leq 0.01$ vs DMSO; ***$p \leq 0.001$ vs DMSO; ****$p \leq 0.0001$ vs DMSO. Table includes reference $IC_{50}$s from RBE assay.

## Conclusion

In this manuscript, we have described the extensive SAR studies that were undertaken around YC-1 to define key structural features that were responsible for its selective cytotoxicity towards mIDH1 expressing cells. During our investigation we discovered that the cytotoxicity was dependent on the expression of the sulfotransferase enzyme SULT1A1, independent of mIDH1 status. We proposed that the furfuryl alcohol served as a novel substrate for SULT1A1 and we proposed a mechanism by which the sulfated species can be eliminated, forming a cationic electrophilic species that bioactivates specific proteins whose alkylation leads to the cytotoxicity.[2] Through the development of a biochemical SULT1A1 colorimetric assay, we were able to directly establish YC-1's role as a substrate for this enzyme. We were also able to ascertain the substrate activity of a class of cytotoxic 4-amino benzyl alcohols and prove that they were superior substrates for SULT1A1 in the biochemical assay. We showed that furfuryl amine replacement for the furfuryl alcohol in YC1, while active in cells, may not be turned over by SULT1A1. These studies, in combination with the assessment of drug-like parameters and pharmacokinetics helped us select YC-1 one as a candidate for in vivo evaluation where it showed efficacy in an immunodeficient mouse SULT1A1-expressing tumor xenograft model. While we were able to dose YC-1 at 50 mpk for several days in the xenograft studies without any signs of toxicity detailed

investigations are required to establish the specificity of the cytotoxic mechanism and establish a carefully titrated safety window for their therapeutic use.

## Methods

### Reagents for SULT1A1 assay

*E. coli*-derived human cytosolic Sulfotransferase 1A1 (SULT1A1) protein Glu2-Leu295 with an N-terminal Met and 6-His tag was obtained from R&D Systems (Cat#: 5546-ST), 4-Nitrophenyl Sulfate (para-nitrophenol sulfate/PNPS) was obtained from Thermo Scientific (CAS#: 6217-68-1, Cat#:227490010), 3'-Phosphoadenosine 5'-Phosphosulfate (PAPS) was used as a sulfate source for SULT1A1 and was obtained from R&D Systems (CAS#4:82-67-7, Cat#:ES019). 2-Napthol was used as a positive control for sulfonation and was obtained from Sigma Aldrich (CAS#:135-19-3, Cat#:185507-100G). 4-Nitrophenol (PNP) was used to generate a curve to directly correlate the absorbance at 405nm with the concentration of PNP formed from sulfonation and was obtained from Sigma Aldrich (CAS#:100-02-7, Cat#:241326-50G). MES monohydrate at pH 7.5 was used as the assay buffer and was obtained from Thermo Scientific (CAS#:145224-94-8, Cat#:J62752.AK). DMSO was used to dissolve small molecules and was obtained from Thermo Scientific (CAS#:67-68-5, Cat#:036480.K2). UltraPure™ DNase/RNase-Free Distilled Water was obtained from Thermo Scientific (CAS#:7732-18-5, Cat#:10977015).

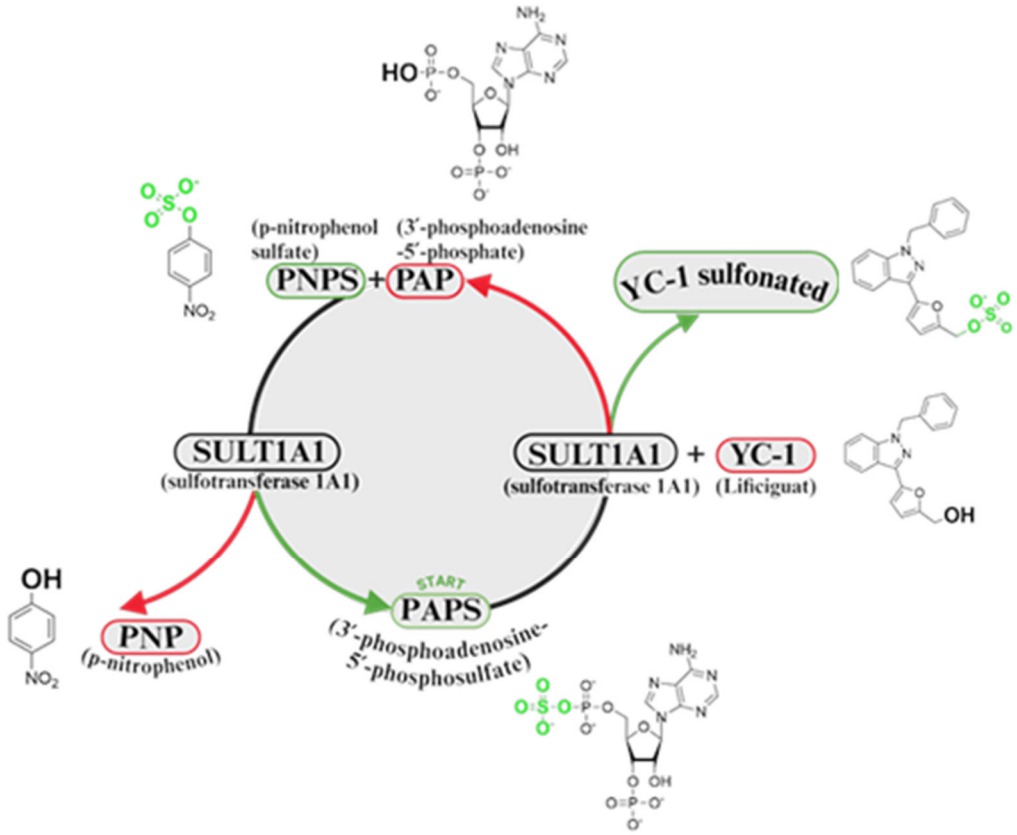


**Figure 6**. Schematic for the colorimetric SULT1A1 activity assay.

### Colorimetric Assay

SULT1A1 activity was measured using a colorimetric assay in which the formation of p-nitrophenol upon the sulfonation of a substrate would correlate directly to sulfonation activity (**Figure 6**).[17] P-Nitrophenol is generated by the desulfonation of p-nitrophenyl sulfate by SULT1A1 to regenerate PAPS thus allowing for more sulfonation of the substrate. P-Nitrophenol has a stable yellow color in solution that can be read at 405 nm on a plate reader. The colorimetric assay quantifying sulfonation of a substrate was originally devised by Mulder at al. 1977.[18]

To make the assay buffer, 1.0 M MES buffer was diluted to 50 mM using UltraPure water. To a 384-well clear bottom black assay plate (Corning® CellBIND® Ref. 3770) was added 9.25 µL of 50 mM MES assay buffer (pH of 7.5) to each well. Then, 5 µL of 1 mM PAPS, which was diluted from a 6.64 mM stock using assay buffer, was added to the wells. Next, the acceptor substrate (YC-1 and analogs) or the positive control (2-Napthol) at 10 mM in DMSO was diluted 20X in the MES assay buffer for a final concentration of 500 µM. Then, 5 µL of the 500 µM acceptor substrate solution was added to the well. After the substrate was added, 5 µL of 5 mM PNPS in assay buffer was added. Finally, the enzymatic reaction was initiated upon addition of 0.75 µL of SULT1A1 (25.1 µM) to the well to give a final SULT1A1 concentration of 0.75 µM and final well volume of 25 µL. The well was pipetted up and down and mixed with the pipette tip. As a negative control (blank), 25 µL of assay buffer was added to a well. The plate was immediately taken to the Tecan Spark® Microplate Reader and absorbance at 405 nm was read for 120 minutes with measurements taken every 5 minutes. Data was graphed and analyzed using the GraphPad Prism software (version 10.2.23).

**Kinetic Solubility Assay**

Pion's patented µSOL assay was used for kinetic solubility determination. In this assay, the classical saturation shake-flask solubility method was adapted as previously described.[19] Test compounds were prepared in 10 mM DMSO stock and diluted to a final drug concentration of 150 µM in the aqueous solution (pH 7.4, 100 mM Phosphate buffer). Samples were incubated at room temperature for 6 hours and vacuum-filtered using Tecan Te-Vac to remove any precipitates. The concentration of the compound in the filtrate was measured via UV absorbance (λ: 250-498 nm). The unknown drug concentration was determined by comparing the fully solubilized reference plate which contained 17 µM of compound dissolved in spectroscopically pure n-propanol. All compounds were tested in duplicates. The kinetic solubility (µg/mL) of compounds was calculated using the µSOL Evolution software. The three controls used were albendazole (low solubility), phenazolpyridine (moderate solubility) and furosemide (high solubility).[20]

**Rat Liver Microsome Stability Assay**

Single time point microsomal stability was determined in a 96-well HTS format. Sample preparation was automated using Tecan EVO 200 robot. High Resolution LC/MS (Thermo QExactive) instrument was used to measure the percentage of compound remaining after incubation using a previously described method.[21] Six standard controls were tested in each run: buspirone and propranolol (for short half-life), loperamide and diclofenac (for short to medium half-life), and carbamazepine and antipyrine (for long half-life). 10 mM DMSO stock solutions of the drugs were first diluted to 10 µM in 1:2 MeCN:DI $H_2O$ and then further diluted to 1 µM in assay buffer. Briefly, the incubation consisted of 0.5 mg/mL microsomal protein, 1.0 µM drug concentration, and NADPH regeneration system (containing 0.650 mM NADP+, 1.65 mM glucose 6-phosphate, 1.65 mM MgCl2, and 0.2 unit/mL G6PDH) in 100 mM phosphate buffer at pH 7.4. The incubation was carried out at 37 °C for 15 min.[22] The reaction was quenched by adding 555

µL of acetonitrile (~1:2 ratio) containing 0.28 µM albendazole (internal standard). Sample acquisition and data analysis was done using a previously described method.[21]

**Parallel Artificial Membrane Permeability Assay (PAMPA)**

Stirring double-sink PAMPA method (patented by pION Inc.) was employed to determine the permeability of compounds via PAMPA as published before.[23] The PAMPA lipid membrane consisted of an artificial membrane of a proprietary lipid mixture and dodecane (Pion Inc.), optimized to predict gastrointestinal tract (GIT) passive permeability. The lipid was immobilized on a plastic matrix of a 96-well "donor" filter plate placed below a 96-well "acceptor" plate. pH 7.4 solution was used in both donor and acceptor wells. The test articles, stocked in 10 mM DMSO solutions, were diluted to 0.05 mM in aqueous buffer (pH 7.4), and the concentration of DMSO was 0.5% in the final solution. During the 30-minute permeation period at room temperature, the test samples in the donor compartment were stirred using the Gutbox technology (Pion Inc.) to reduce the aqueous boundary layer. The test article concentrations in the donor and acceptor compartments were measured using a UV plate reader (Nano Quant, Infinite® 200 PRO, Tecan Inc., Männedorf, Switzerland). Permeability calculations were performed using Pion Inc. software and were expressed in units of 10-6cm/s. Compounds with low or weak UV signal we analyzed using high resolution LC/MS (Thermo QExactive). The three controls used were ranitidine (low permeability), dexamethasone (moderate permeability) and verapamil (high permeability).

**Mouse Pharmacokinetic Studies**. Studies were conducted by Pharmaron. Fed male CD1 mice (sourced from Si Bei Fu LaboratoryAnimal Technology Co. Ltd.), approximately 6−8 weeks of age and weight of approximately 25−30 g, were dosed with compounds **1**, **15** and **58**. The formulation for **58** was 5% NMP, 20% PEG 300, 75% "solutol HS 15 in water (15 wt%)" and the dosing concentration was 2.5, 1, 3 mg/mL for the 5, 10 , 30 mpk IV, PO and IP experiments at dosing volume 2, 10 and 10 mL/kg respectively. The formulation for compounds **1** and **15** was PEG300 / 30% solutol in water / Saline (30/17/54) as 1, 1, 3 mg/mL for the 5, 10, 30 mpk doses. Formulated drug samples were prepared prior to dosing a cohort of N=3 mice in each arm. 25 µL of blood was collected from the dorsal metatarsal vein by serial bleeding. Blood samples were then transferred into plastic microcentrifuge tubes containing heparin−Na as anticoagulant. Samples were then centrifuged at 4000g for 5 min at 4°C to obtain plasma. Plasma samples were then stored in polypropylene tubes, quickly frozen, and kept at−75°C until analyzed by LC/MS/MS. Animals were also monitored during the in-life phase by once daily cageside observations; no adverse clinical signs were noted as part of the PK report.

**Use of Animal Subjects**. All animal studies included as part of this manuscript were performed in accordance with institutional guidelines as defined by Institutional Animal Care and Use Committee (IACUC).

**Cell Titer Glo Assay Protocol**

| Step | | Value | Description |
|---|---|---|---|
| 1 | Cell Addition | 5 µL | Cells in culture medium |
| 2 | Compound Addition | 23 nL | Dilution series |
| 3 | Incubation | 72 hr | 37 °C, 5% $CO_2$, 85% RH |
| 4 | CellTiter-Glo Reagent Addition | 2.5 µL | CellTiter-Glo Reagent Addition |
| 5 | Incubation | 10 mins | Room temperature |

| | | | |
|---|---|---|---|
| 6 | Detection | Luminescence | ViewLux, 1 sec exposure |

| Notes | |
|---|---|
| 1 | Cells were cultured in RPMI 1640 (Life Technologies) supplemented with 10% fetal bovine serum (FBS; HyClone), 100 U/ml penicillin and 100 µg/ml streptomycin. |
| 2 | Pintool transfer |
| 3 | 37 °C, 5% $CO_2$, 85% RH incubator incubation for 72 hr treatment conditions |
| 4 | CellTiter-Glo (Promega) reagent quantifies cellular ATP levels as a proxy for viability |

## Experimental Section Chemistry

### General Methods for Chemistry.

All air- or moisture-sensitive reactions were performed under positive pressure of nitrogen with oven-dried glassware. Anhydrous solvents or reagents such as dichloromethane, *N,N*-dimethylformamide (DMF), acetonitrile, methanol, and triethylamine were purchased from Sigma-Aldrich. To follow most chemical reactions LC/MS of reaction aliquots were analyzed using a gradient of 4% to 100% acetonitrile (containing 0.025% trifluoroacetic acid) and water (containing 0.05% trifluoroacetic acid) with a 4.5-minute run time at a flow rate of 1 mL/min in an Agilent Extend-C18 column (3.5 micron, 4.6 x 100 mm) at a temperature of 50 °C using an Agilent Diode Array Detector. Confirmation of molecular formulae was accomplished using electrospray ionization in the positive mode with the Agilent Masshunter software (version B.02).

**Preparative purification** was performed on a Waters semi-preparative HPLC system. The column used was a Phenomenex Luna C18 (5 micron, 30 x 75 mm) at a flow rate of 45 mL/min. The mobile phase consisted of acetonitrile and water (each containing 0.1% trifluoroacetic acid). A gradient of 10% to 50% acetonitrile over 8 minutes was used during the purification. Fraction collection was triggered by UV detection (220 nM).

**Purity** of all final compounds was ≥95% as determined on an Agilent LC/MS (Agilent Technologies, Santa Clara, CA) using a 7-minute gradient of 4% to 100% acetonitrile (containing 0.025% trifluoroacetic acid) and water (containing 0.05% trifluoroacetic acid) with an 8-minute run time at a flow rate of 1 mL/min. A Phenomenex Luna C18 column (3 micron, 3 x 75 mm) was used at a temperature of 50 °C using an Agilent Diode Array Detector. Mass determination was performed using an Agilent 6130 mass spectrometer with electrospray ionization in the positive mode.

$^1$H NMR spectra were recorded on Varian 400 MHz spectrometers. Chemical shifts are reported in ppm with non-deuterated solvent (DMSO-$h_6$ at 2.50 ppm) as internal standard for DMSO-$d_6$ solutions.

### Compound Characterization

**(5-(1-benzyl-1H-indazol-3-yl)furan-2-yl)methanol (1)**
LCMS: m/z (M + H)+ = 305.1, $^1$H NMR (400 MHz, $CDCl_3$) δ 8.06 (dt, J = 1.0, 8.2 Hz, 1H), 7.39 – 7.17 (m, 8H), 6.87 (d, J = 3.3 Hz, 1H), 6.50 – 6.45 (m, 1H), 5.65 (s, 2H), 4.75 (d, J = 6.2 Hz, 2H), 1.89 (t, J = 6.3 Hz, 1H).
**2-(5-(1-benzyl-1H-indazol-3-yl)furan-2-yl)ethan-1-ol (2)**
LCMS: m/z (M + H)+ = 319.0.
**1-benzyl-3-(5-(methoxymethyl)furan-2-yl)-1H-indazole (3)**

LCMS: m/z (M + H)+ = 319.1, $^1$H NMR (400 MHz, $CDCl_3$) δ 8.11 (dt, J = 1.0, 8.2 Hz, 1H), 7.36 – 7.19 (m, 8H), 6.88 (d, J = 4.0 Hz, 1H), 6.5 (d,J = 4.0Hz 1H), 5.65 (s, 2H), 4.54 (s, 2H), 3.43 (s, 3H).

**1-benzyl-3-(5-methylfuran-2-yl)-1H-indazole (4)**

LCMS: m/z (M + H)+ = 289.1, ($^1$H NMR (400 MHz, $CDCl_3$) δ 8.04 (dt, J = 1.1, 8.0 Hz, 1H), 7.36 – 7.16 (m, 8H), 7.25 (s, 6H), 6.81 (d, J = 3.2 Hz, 1H), 6.18 – 6.12 (m, 1H), 5.65 (s, 2H), 5.29 (d, J = 0.4 Hz, 1H), 2.45 (d, J = 1.0 Hz, 3H).

**1-(5-(1-benzyl-1H-indazol-3-yl)furan-2-yl)ethan-1-ol (5)**

LCMS: m/z (M + H)+ = 319.2.

**1-(5-(1-benzyl-1H-indazol-3-yl)furan-2-yl)cyclopropan-1-ol (6)**

LCMS: m/z (M + H)+ = 331.1, $^1$H NMR (400 MHz, $CDCl_3$) δ 8.02 (dt, J = 1.1, 8.2 Hz, 1H), 7.42 – 7.15 (m, 8H), 6.87 (d, J = 3.3 Hz, 1H), 6.39 (d, J = 3.3 Hz, 1H), 5.64 (s, 2H), 1.23 (dt, J = 1.6, 7.1 Hz, 4H).

**(2-(1-benzyl-1H-indazol-3-yl)oxazol-5-yl)methanol (7)**

LCMS: m/z (M + H)+ = 306.1, $^1$H NMR (400 MHz, $CD_3OD$) δ 8.29 (dd, J = 1.3, 8.1 Hz, 1H), 7.62 (dd, J = 0.8, 8.5 Hz, 1H), 7.50 – 7.42 (m, 1H), 7.36 – 7.21 (m, 7H), 5.73 (s, 2H), 4.72 (s, 2H).

**(5-(1-benzyl-1H-indazol-3-yl)oxazol-2-yl)methanol (8)**

LCMS: m/z (M + H)+ = 306.1

**(2-(1-benzyl-1H-indazol-3-yl)oxazol-4-yl)methanol (9)**

LCMS: m/z (M + H)+ = 306 , $^1$H NMR (400 MHz, $CD_3OD$) δ 8.29 (dq, J = 1.0, 8.3 Hz, 1H), 7.94 (d, J = 1.1 Hz, 1H), 7.59 (dd, J = 1.1, 8.6 Hz, 1H), 7.49 – 7.40 (m, 1H), 7.35 – 7.25 (m, 3H), 7.29 – 7.19 (m, 3H), 5.72 (s, 2H), 4.64 (d, J = 1.0 Hz, 2H).

**(5-(1-benzyl-1H-indazol-3-yl)thiophen-2-yl)methanol (10)**

LCMS: m/z (M + H)+ = 321.1 , $^1$H NMR (400 MHz, $CDCl_3$) δ 7.97 (dt, J = 1.0, 8.2 Hz, 1H), 7.74 (d, J = 1.4 Hz, 1H), 7.64 (dd, J = 0.8, 1.5 Hz, 1H), 7.40 – 7.28 (m, 2H), 7.32 – 7.19 (m, 4H), 7.23 – 7.16 (m, 2H), 5.62 (s, 2H), 5.29 (s, 1H), 4.90 (d, J = 0.9 Hz, 2H).

**(3-(1-benzyl-1H-indazol-3-yl)phenyl)methanol (11)**

LCMS: m/z (M + H)+ = 315.1 , $^1$H NMR (400 MHz, $CDCl_3$) δ 8.06 – 7.96 (m, 2H), 7.91 (dt, J = 1.5, 7.7 Hz, 1H), 7.50 (t, J = 7.6 Hz, 1H), 7.43 – 7.17 (m, 9H), 5.66 (s, 2H), 4.80 (s, 2H), 1.84 (s, 1H).

**(5-(1-benzyl-1H-indazol-3-yl)tetrahydrofuran-2-yl)methanol (12)**

LCMS: m/z (M + H)+ = 309.2

**(5-(1-benzyl-1H-indazol-3-yl)furan-2-yl)methyl isobutyrate (13)**

LCMS: m/z (M + H)+ = 375.1, $^1$H NMR (400 MHz, $CDCl_3$) δ 8.08 (dt, *J* = 1.0, 8.2 Hz, 1H), 7.39 – 7.29 (m, 5H), 7.24 – 7.19 (m, 3H), 6.89 (d, *J* = 3.3 Hz, 1H), 6.56 (dd, *J* = 0.5, 3.4 Hz, 1H), 5.65 (s, 2H), 5.19 (s, 2H), 2.65 – 2.55 (m, 1H), 1.18 (d, *J* = 7.0 Hz, 6H).

**ethyl 5-(1-benzyl-1H-indazol-3-yl)furan-2-carboxylate (14)**

LCMS: m/z (M + H)+ = 347.2 , $^1$H NMR (400 MHz, $CDCl_3$) δ 8.25 (dt, J = 1.0, 8.2 Hz, 1H), 7.41 – 7.17 (m, 9H), 7.00 (d, J = 3.6 Hz, 1H), 5.64 (s, 2H), 4.40 (q, J = 7.0 Hz, 2H), 1.41 (t, J = 7.1 Hz, 3H).

**(5-(1-benzyl-1H-indazol-3-yl)furan-2-yl)methanamine (15)**

LCMS: m/z (M + H)+ = 304.1 , $^1$H NMR (400 MHz, $CD_3OD$) δ 8.16 (dt, J = 1.0, 8.3 Hz, 1H), 7.56 (dt, J = 0.9, 8.6 Hz, 1H), 7.49 – 7.40 (m, 1H), 7.33 – 7.20 (m, 4H), 7.19 (dd, J = 1.7, 8.0 Hz, 2H), 7.01 (d, J = 3.4 Hz, 1H), 6.75 – 6.70 (m, 1H), 5.67 (s, 2H), 4.29 (s, 2H).

**1-(5-(1-benzyl-1H-indazol-3-yl)furan-2-yl)-N-methylmethanamine (16)**

LCMS: m/z (2M + H)+ = 635.4, $^1$H NMR (400 MHz, $CDCl_3$) δ 8.07 (dd, J = 1.0, 8.2 Hz, 1H), 7.39 – 7.17 (m, 8H), 6.87 (d, J = 3.3 Hz, 1H), 6.48 (t, J = 2.8 Hz, 1H), 5.64 (s, 2H), 4.03 – 3.97 (m, 2H), 2.53 (s, 2H), 2.02 (m, 3H).

**N-((5-(1-benzyl-1H-indazol-3-yl)furan-2-yl)methyl)hydroxylamine (17)**

LCMS: m/z (M + H)+ = 320.2, $^1$H NMR (400 MHz, $CD_3OD$) δ 8.15 (dt, *J* = 1.0, 8.2 Hz, 1H), 7.57 – 7.34 (m, 2H), 7.31 – 7.14 (m, 6H), 7.04 – 6.89 (m, 1H), 6.49 (d, *J* = 3.3 Hz, 1H), 5.63 (s, 2H), 4.09 (s, 2H)

**(5-(1H-indazol-3-yl)furan-2-yl)methanol (18)**

LCMS: m/z (M + H)+ = 215.1.

**(5-(1-methyl-1H-indazol-3-yl)furan-2-yl)methanol (19)**

LCMS: m/z (M + H)+ = 229.1, $^1$H NMR (400 MHz, $CD_3OD$) δ 8.11 (dt, J = 1.0, 8.3 Hz, 1H), 7.51 (dt, J = 1.0, 8.5 Hz, 1H), 7.43 (ddd, J = 1.1, 6.8, 8.6 Hz, 1H), 7.25 – 7.19 (m, 1H), 6.86 (d, J = 3.3 Hz, 1H), 6.46 (dt, J = 0.6, 3.4 Hz, 1H), 4.62 (s, 2H), 4.05 (s, 3H).

**(5-(1-(2-methylallyl)-1H-indazol-3-yl)furan-2-yl)methanol (20)**

LCMS: m/z (M + H)+ = 269.2, $^1$H NMR (400 MHz, $CD_3OD$) δ 8.15 (d, J = 8.2 Hz, 1H), 7.55 – 7.38 (m, 2H), 7.28 – 7.20 (m, 1H), 6.90 (d, J = 3.4 Hz, 1H), 6.48 (d, J = 3.3 Hz, 1H), 5.00 (s, 2H), 4.91 (s, 1H), 4.69 (s, 1H), 4.63 (s, 1H), 1.66 (s, 3H).

**(5-(1-(cyclohexylmethyl)-1H-indazol-3-yl)furan-2-yl)methanol (21)**

LCMS: m/z (M + H)+ = 311.1.

**(5-(1-phenyl-1H-indazol-3-yl)furan-2-yl)methanol (22)**

LCMS: m/z (M + H)+ = 291.0, $^1$H NMR (400 MHz, $CD_3OD$) δ 8.24 (dq, J = 0.9, 8.2 Hz, 1H), 7.77 – 7.69 (m, 3H), 7.60 – 7.55 (m, 2H), 7.51 – 7.46 (m, 1H), 7.43 – 7.39 (m, 1H), 7.31 (ddt, J = 0.7, 6.9, 8.3 Hz, 1H), 7.00 (d, J = 3.2 Hz, 1H), 6.51 (dt, J = 0.6, 3.4 Hz, 1H), 4.65 (s, 2H).

**(5-(1-phenethyl-1H-indazol-3-yl)furan-2-yl)methanol (23)**

LCMS: m/z (M + H)+ = 319.2 , $^1$H NMR (400 MHz, cd3od) δ 8.06 (dt, J = 1.0, 8.2 Hz, 1H), 7.34 – 7.19 (m, 2H), 7.18 – 7.00 (m, 6H), 6.88 (t, J = 3.7 Hz, 1H), 6.47 (d, J = 3.3 Hz, 1H), 4.70 – 4.54 (m, 4H), 3.17 (q, J = 9.6 Hz, 2H).

**(3-(5-(hydroxymethyl)furan-2-yl)-1H-indazol-1-yl)(phenyl)methanone (24)**

LCMS: m/z (M + H)+ = 319.1.

**(5-(1-(phenylsulfonyl)-1H-indazol-3-yl)furan-2-yl)methanol (25)**

LCMS: m/z (M + H)+ = 355.1, $^1$H NMR (400 MHz, $CD_3OD$) δ 8.24 – 8.16 (m, 2H), 7.99 – 7.92 (m, 2H), 7.69 – 7.55 (m, 2H), 7.55 – 7.45 (m, 2H), 7.48 – 7.39 (m, 1H), 7.15 (dd, J = 1.1, 3.4 Hz, 1H), 6.51 (d, J = 3.4 Hz, 1H), 4.63 (s, 2H).

**benzyl 3-(5-(hydroxymethyl)furan-2-yl)-1H-indazole-1-carboxylate (26)**

LCMS: m/z (M + H)+ = 349.1 , $^1$H NMR (400 MHz, $CDCl_3$) δ 8.23 (d, J = 8.5 Hz, 1H), 8.14 (dt, J = 1.0, 8.1 Hz, 1H), 7.59 – 7.53 (m, 3H), 7.43 – 7.35 (m, 4H), 7.12 (d, J = 3.4 Hz, 1H), 6.50 (d, J = 3.4 Hz, 1H), 5.58 (s, 2H), 4.76 (s, 2H).

**(5-(1-(1-phenylethyl)-1H-indazol-3-yl)furan-2-yl)methanol (27)**

LCMS: m/z (M + H)+ = 319.2 **,** $^1$H NMR (400 MHz, $CD_3OD$) δ 8.12 (dt, J = 1.0, 8.2 Hz, 1H), 7.41 (dt, J = 1.0, 8.7 Hz, 1H), 7.35 – 7.29 (m, 1H), 7.27 – 7.18 (m, 4H), 7.22 – 7.12 (m, 2H), 6.90 (d, J = 3.3 Hz, 1H), 6.52 – 6.45 (m, 1H), 5.94 (q, J = 7.0 Hz, 1H), 4.64 (s, 2H), 2.01 (d, J = 7.0 Hz, 3H).

**(5-(1-(2-fluorobenzyl)-1H-indazol-3-yl)furan-2-yl)methanol (28)**

LCMS: m/z (M + H)+ = 323.1, $^1$H NMR (400 MHz, $CD_3OD$) δ 8.16 (dt, J = 1.1, 8.3 Hz, 1H), 7.54 (d, J = 8.5 Hz, 1H), 7.44 (dd, J = 1.2, 6.9 Hz, 1H), 7.30 – 7.19 (m, 2H), 7.12 (s, 1H), 7.08 –

7.00 (m, 2H), 6.91 (d, J = 3.3 Hz, 1H), 6.48 (d, J = 3.3 Hz, 1H), 5.70 (s, 2H), 4.63 (s, 2H). $^{19}$F NMR (376 MHz, $CD_3OD$) δ -120.28

**(5-(1-(3-fluorobenzyl)-1H-indazol-3-yl)furan-2-yl)methanol (29)**

LCMS: m/z (M + H)+ = 323.1, $^1$H NMR (400 MHz, $CD_3OD$) δ 8.15 (dt, J = 1.0, 8.2 Hz, 1H), 7.49 (dt, J = 0.9, 8.5 Hz, 1H), 7.41 (m, 1H), 7.31 – 7.20 (m, 2H), 7.02 – 6.88 (m, 4H), 6.47 (d, J = 3.3 Hz, 1H), 4.82 (s, 2H), 4.63 (s, 2H). $^{19}$F NMR (376 MHz, $CD_3OD$) δ -114.81

**(5-(1-(4-fluorobenzyl)-1H-indazol-3-yl)furan-2-yl)methanol (30)**

LCMS: m/z (M + H)+ = 323.0, $^1$H NMR (400 MHz, $CDCl_3$) δ 8.05 (dt, J = 0.9, 8.2 Hz, 1H), 7.39 – 7.34 (m, 1H), 7.29 (dq, J = 0.9, 8.5 Hz, 1H), 7.24 – 7.16 (m, 4H), 7.00 – 6.93 (m, 2H), 6.87 (d, J = 3.3 Hz, 1H), 6.47 (d, J = 3.3 Hz, 1H), 5.60 (s, 2H), 4.74 (s, 2H). $^{19}$F NMR (376 MHz, $CD_3OD$) δ -114.48

**(5-(1-(2-chlorobenzyl)-1H-indazol-3-yl)furan-2-yl)methanol (31)**

LCMS: m/z (M + H)+ = 339.1, $^1$H NMR (400 MHz, $CD_3OD$) δ 8.23 – 8.12 (m, 1H), 7.48 (d, J = 8.6 Hz, 1H), 7.47 – 7.34 (m, 2H), 7.25 (tt, J = 3.2, 8.1 Hz, 2H), 7.15 (dd, J = 6.7, 8.2 Hz, 1H), 6.91 (dd, J = 1.5, 3.3 Hz, 1H), 6.72 (d, J = 7.7 Hz, 1H), 6.48 (dd, J = 1.4, 3.5 Hz, 1H), 5.76 (s, 2H), 4.63 (s, 2H).

**(5-(1-(3-chlorobenzyl)-1H-indazol-3-yl)furan-2-yl)methanol (32)**

LCMS: m/z (M + H)+ = 339.1, $^1$H NMR (400 MHz, $CD_3OD$) δ 8.17 (dt, J = 1.0, 8.3 Hz, 1H), 7.53 (dd, J = 1.1, 8.6 Hz, 1H), 7.48 – 7.40 (m, 1H), 7.28 – 7.21 (m, 4H), 7.12 (d, J = 6.4 Hz, 1H), 6.92 (d, J = 3.4 Hz, 1H), 6.49 (d, J = 3.4 Hz, 1H), 5.64 (s, 2H), 4.64 (s, 2H).

**(5-(1-(4-chlorobenzyl)-1H-indazol-3-yl)furan-2-yl)methanol (33)**

LCMS: m/z (M + H)+ = 339.1, $^1$H NMR (400 MHz, $CD_3OD$) δ 8.14 (dt, J = 1.0, 8.2 Hz, 1H), 7.48 (dd, J = 1.0, 8.6 Hz, 1H), 7.39 (td, J = 1.1, 6.8 Hz, 1H), 7.29 – 7.08 (m, 6H), 6.89 (d, J = 3.3 Hz, 1H), 6.51 – 6.44 (m, 1H), 5.59 (s, 2H), 4.62 (s, 2H).

**(5-(1-(2-methylbenzyl)-1H-indazol-3-yl)furan-2-yl)methanol (34)**

LCMS: m/z (M + H)+ = 319.2, $^1$H NMR (400 MHz, $CD_3OD$) δ 8.15 (dd, J = 1.2, 8.2 Hz, 1H), 7.37 – 7.32 (m, 2H), 7.26 – 7.16 (m, 1H), 7.18 – 7.08 (m, 2H), 7.01 (t, J = 7.1 Hz, 1H), 6.88 (d, J = 3.3 Hz, 1H), 6.68 (d, J = 7.7 Hz, 1H), 6.46 (d, J = 3.3 Hz, 1H), 5.60 (s, 2H), 4.62 (s, 2H), 2.32 (s, 3H).

**(5-(1-(3-methylbenzyl)-1H-indazol-3-yl)furan-2-yl)methanol (35)**

LCMS: m/z (M + H)+ = 319.2 Sample order for NMR

**(5-(1-(4-methylbenzyl)-1H-indazol-3-yl)furan-2-yl)methanol (36)**

LCMS: m/z (M + H)+ = 319.2, $^1$H NMR (400 MHz, $CD_3OD$) δ 8.14 (d, J = 8.2 Hz, 1H), 7.49 (d, J = 8.5 Hz, 1H), 7.39 (dd, J = 7.0, 8.2 Hz, 1H), 7.22 (t, J = 7.5 Hz, 1H), 7.09 (s, 4H), 6.90 (d, J = 3.4 Hz, 1H), 6.48 (d, J = 3.3 Hz, 1H), 5.59 (d, J = 3.5 Hz, 2H), 4.63 (s, 2H), 2.26 (s, 3H).

**(5-(1-(2-methoxybenzyl)-1H-indazol-3-yl)furan-2-yl)methanol (37)**

LCMS: m/z (M + H)+ = 335.1, $^1$H NMR (400 MHz, $CD_3OD$) δ 8.14 (d, J = 8.2 Hz, 1H), 7.53 – 7.36 (m, 2H), 7.23 (s, 2H), 6.98 (d, J = 8.3 Hz, 1H), 6.89 (d, J = 3.4 Hz, 1H), 6.80 (d, J = 4.6 Hz, 2H), 6.47 (d, J = 3.3 Hz, 1H), 5.62 (s, 2H), 4.63 (s, 2H), 3.85 (s, 3H).

**(5-(1-(3-methoxybenzyl)-1H-indazol-3-yl)furan-2-yl)methanol (38)**

LCMS: m/z (M + H)+ = 335.1, $^1$H NMR (400 MHz, $CDCl_3$) δ 8.04 (dt, J = 1.2, 8.0 Hz, 1H), 7.38 – 7.28 (m, 2H), 7.24 – 7.16 (m, 2H), 6.89 – 6.85 (m, 1H), 6.81 – 6.76 (m, 2H), 6.74 (t, J = 2.1 Hz, 1H), 6.46 (ddt, J = 0.7, 1.8, 3.2 Hz, 1H), 5.61 (s, 2H), 4.74 (s, 2H), 3.71 (s, 3H).

**(5-(1-(4-methoxybenzyl)-1H-indazol-3-yl)furan-2-yl)methanol (39)**

LCMS: m/z (M + H)+ = 335.0.

**(5-(1-(pyridin-2-ylmethyl)-1H-indazol-3-yl)furan-2-yl)methanol (40)**
LCMS: m/z (M + H)+ = 306.1.
**(5-(1-(pyridin-3-ylmethyl)-1H-indazol-3-yl)furan-2-yl)methanol (41)**
LCMS: m/z (M + H)+ = 306.1, $^1$H NMR (400 MHz, $CD_3OD$) δ 8.47 (d, J = 2.3 Hz, 1H), 8.44 – 8.38 (m, 1H), 8.14 (dt, J = 1.0, 8.2 Hz, 1H), 7.66 (dt, J = 2.1, 7.9 Hz, 1H), 7.57 (dt, J = 1.0, 8.6 Hz, 1H), 7.43 (tt, J = 1.0, 7.9 Hz, 1H), 7.33 (dd, J = 4.9, 8.0 Hz, 1H), 7.23 (dd, J = 6.9, 8.1 Hz, 1H), 6.90 (d, J = 3.3 Hz, 1H), 6.47 (d, J = 3.4 Hz, 1H), 5.68 (s, 2H), 4.62 (s, 2H).
**(5-(1-(pyridin-4-ylmethyl)-1H-indazol-3-yl)furan-2-yl)methanol (42)**
LCMS: m/z (M + H)+ = 306.1.
**(5-(1-(pyrimidin-5-ylmethyl)-1H-indazol-3-yl)furan-2-yl)methanol (43)**
LCMS: m/z (M + H)+ = 307.1, $^1$H NMR (400 MHz, $CD_3OD$) δ 9.03 (s, 1H), 8.70 (s, 2H), 8.15 (dt, J = 1.0, 8.2 Hz, 1H), 7.63 (dt, J = 0.9, 8.5 Hz, 1H), 7.46 (ddd, J = 1.1, 6.9, 8.5 Hz, 1H), 7.29 – 7.19 (m, 1H), 6.90 (d, J = 3.4 Hz, 1H), 6.47 (dt, J = 0.6, 3.4 Hz, 1H), 5.70 (s, 2H), 4.63 (s, 2H).
**(5-(1-((5-methylthiazol-2-yl)methyl)-1H-indazol-3-yl)furan-2-yl)methanol (44)**
LCMS: m/z (M + H)+ = 326.1, $^1$H NMR (400 MHz, $CD_3OD$) δ 8.20 – 8.13 (m, 1H), 7.59 (d, J = 8.5 Hz, 1H), 7.48 – 7.36 (m, 2H), 7.26 (dd, J = 7.0, 8.1 Hz, 1H), 6.93 (d, J = 3.3 Hz, 1H), 6.48 (d, J = 3.4 Hz, 1H), 5.86 (s, 2H), 4.63 (s, 2H), 2.36 (d, J = 1.2 Hz, 3H).
**(5-(1-((3-methoxypyridin-4-yl)methyl)-1H-indazol-3-yl)furan-2-yl)methanol (45)**
LCMS: m/z (M + H)+ = 336.2, $^1$H NMR (400 MHz, $CD_3OD$) δ 8.34 (d, J = 5.8 Hz, 1H), 8.14 (dd, J = 1.1, 8.2 Hz, 1H), 8.01 (s, 1H), 7.59 (d, J = 8.5 Hz, 1H), 7.45 (ddd, J = 1.1, 6.9, 8.5 Hz, 1H), 7.28 – 7.20 (m, 1H), 7.06 (d, J = 5.8 Hz, 1H), 6.89 (d, J = 3.3 Hz, 1H), 6.47 (d, J = 3.3 Hz, 1H), 5.63 (s, 2H), 4.62 (s, 2H), 3.91 (s, 3H).
**(5-(1-((2-methoxypyridin-4-yl)methyl)-1H-indazol-3-yl)furan-2-yl)methanol (46)**
LCMS: m/z (M + H)+ = 336.2, $^1$H NMR (400 MHz, $CD_3OD$) δ 8.16 (dt, J = 1.0, 8.2 Hz, 1H), 7.98 (dd, J = 0.7, 5.4 Hz, 1H), 7.47 (dt, J = 1.0, 8.6 Hz, 1H), 7.44 – 7.39 (m, 1H), 7.24 (ddd, J = 1.1, 6.7, 8.0 Hz, 1H), 6.92 (d, J = 3.3 Hz, 1H), 6.68 (dd, J = 1.5, 5.4 Hz, 1H), 6.51 – 6.45 (m, 2H), 5.61 (s, 2H), 4.63 (s, 2H), 3.81 (s, 3H).
**(5-(1-((2-methoxypyridin-3-yl)methyl)-1H-indazol-3-yl)furan-2-yl)methanol (47)**
LCMS: m/z (M + H)+ = 336.2, $^1$H NMR (400 MHz, $CD_3OD$) δ 8.14 (dt, J = 1.0, 8.2 Hz, 1H), 8.01 (dd, J = 1.9, 5.1 Hz, 1H), 7.51 (dt, J = 1.0, 8.6 Hz, 1H), 7.41 (ddd, J = 1.1, 6.9, 8.4 Hz, 1H), 7.22 (ddd, J = 1.0, 6.9, 8.0 Hz, 1H), 7.14 – 7.07 (m, 1H), 6.88 (d, J = 3.3 Hz, 1H), 6.79 (dd, J = 5.0, 7.3 Hz, 1H), 6.46 (d, J = 3.3 Hz, 1H), 5.56 (s, 2H), 4.62 (s, 2H), 3.94 (s, 3H).

**N-(2-(2-(2-(3-((3-(5-(hydroxymethyl)furan-2-yl)-1H-indazol-1-yl)methyl)phenoxy)ethoxy)ethoxy)ethyl)-5-((3aR,4R,6aS)-2-oxohexahydro-1H-thieno[3,4-d]imidazol-4-yl)pentanamide (48)**
LCMS: m/z (M + H)+ = 678.2, $^1$H NMR (400 MHz, $CD_3OD$) δ 8.15 (dt, J = 1.0, 8.2 Hz, 1H), 7.50 (dt, J = 0.9, 8.5 Hz, 1H), 7.40 (ddd, J = 1.1, 6.9, 8.6 Hz, 1H), 7.26 – 7.17 (m, 2H), 6.92 (d, J = 3.3 Hz, 1H), 6.85 – 6.79 (m, 2H), 6.77 – 6.72 (m, 1H), 6.48 (dd, J = 0.6, 3.4 Hz, 1H), 5.61 (s, 2H), 4.63 (t, J = 0.5 Hz, 2H), 4.38 (ddd, J = 0.9, 5.0, 7.8 Hz, 1H), 4.17 (dd, J = 4.4, 7.9 Hz, 1H), 4.03 – 3.98 (m, 2H), 3.77 – 3.72 (m, 2H), 3.63 – 3.58 (m, 2H), 3.58 – 3.51 (m, 2H), 3.47 (dd, J = 5.0, 5.7 Hz, 2H), 3.30 – 3.27 (m, 3H), 3.05 (ddd, J = 4.4, 5.9, 8.8 Hz, 1H), 2.82 (dd, J = 5.0, 12.8 Hz, 1H), 2.11 (t, J = 7.4 Hz, 2H), 1.63 – 1.51 (m, 3H), 1.31 (dt, J = 7.6, 15.4 Hz, 3H).
**(5-(1-benzyl-1H-pyrazolo[4,3-b]pyridin-3-yl)furan-2-yl)methanol (49)**

LCMS: m/z (M + H)+ = 306.1, $^1$H NMR (400 MHz, $CD_3OD$) δ 8.57 (d, J = 4.6 Hz, 1H), 8.01 (t, J = 7.4 Hz, 1H), 7.41 (dt, J = 5.1, 8.6 Hz, 1H), 7.26 (td, J = 8.2, 14.6 Hz, 6H), 6.50 (t, J = 5.0 Hz, 1H), 5.70 – 5.63 (m, 2H), 4.63 (d, J = 5.1 Hz, 2H).

**(5-(1-benzyl-1H-pyrazolo[4,3-c]pyridin-3-yl)furan-2-yl)methanol (50)**

LCMS: m/z (M + H)+ = 306.0, $^1$H NMR (400 MHz, $CD_3OD$) δ 9.43 (d, J = 1.2 Hz, 1H), 8.34 (d, J = 6.2 Hz, 1H), 7.58 (dd, J = 1.2, 6.2 Hz, 1H), 7.34 – 7.23 (m, 5H), 7.03 (d, J = 3.4 Hz, 1H), 6.51 (d, J = 3.3 Hz, 1H), 5.67 (s, 2H), 4.65 (s, 2H).

**(5-(1-benzyl-1H-pyrazolo[3,4-c]pyridin-3-yl)furan-2-yl)methanol (51)**

LCMS: m/z (M + H)+ = 306.2, $^1$H NMR (400 MHz, $CD_3OD$) δ 9.00 – 8.95 (s, 1H), 8.27 (dd, J = 1.2, 5.7 Hz, 1H), 8.15 (dt, J = 1.3, 5.8 Hz, 1H), 7.36 – 7.23 (m, 5H), 6.97 (dd, J = 1.2, 3.4 Hz, 1H), 6.53 – 6.47 (m, 1H), 5.77 (s, 2H), 4.64 (s, 2H).

**(5-(1-benzyl-1H-pyrazolo[3,4-b]pyridin-3-yl)furan-2-yl)methanol (52)**

LCMS: m/z (M + H)+ = 306.0, $^1$H NMR (400 MHz, $CD_3OD$) δ 8.64 – 8.56 (m, 2H), 7.35 – 7.19 (m, 5H), 6.95 (d, J = 3.4 Hz, 1H), 6.49 (d, J = 3.3 Hz, 1H), 5.72 (s, 2H), 4.64 (s, 2H).

**(5-(1-benzyl-4-chloro-1H-indazol-3-yl)furan-2-yl)methanol (53)**

LCMS: m/z (M + H)+ = 339.1, $^1$H NMR (400 MHz, $CD_3OD$) δ 7.50 (dd, J = 0.8, 8.5 Hz, 1H), 7.37 – 7.16 (m, 7H), 6.83 (d, J = 3.3 Hz, 1H), 6.45 (d, J = 3.3 Hz, 1H), 5.66 (s, 2H), 4.60 (s, 2H).

**(5-(1-benzyl-5-fluoro-1H-indazol-3-yl)furan-2-yl)methanol (54)**

LCMS: m/z (M + H)+ = 323.1, $^1$H NMR (400 MHz, $CD_3OD$) δ 7.80 (dt, J = 2.0, 8.9 Hz, 1H), 7.52 – 7.43 (m, 1H), 7.31 – 7.14 (m, 6H), 6.86 (dd, J = 1.4, 3.4 Hz, 1H), 6.46 (dd, J = 1.4, 3.3 Hz, 1H), 4.85 – 4.80 (m, 2H), 4.62 (s, J = 1.5 Hz, 2H), $^{19}$F NMR (376 MHz, $CD_3OD$) δ -123.74.

**(5-(1-benzyl-1H-indol-3-yl)furan-2-yl)methanol (55)**

Mol mass didn't observe. $^1$H NMR (400 MHz, $CDCl_3$) δ 7.98 – 7.88 (m, 1H), 7.30 (dq, J = 3.0, 5.4 Hz, 2H), 7.30 – 7.21 (m, 3H), 7.24 – 7.09 (m, 4H), 6.47 (d, J = 3.3 Hz, 1H), 6.39 (d, J = 3.2 Hz, 1H), 5.32 (s, 2H), 4.65 (s, 2H) .

**(5-(1-benzyl-4,5,6,7-tetrahydro-1H-indazol-3-yl)furan-2-yl)methanol (56)**

LCMS: m/z (M + H)+ = 309.2, $^1$H NMR (400 MHz, $CD_3OD$) δ 7.32 – 7.20 (m, 3H), 7.12 – 7.07 (m, 2H), 6.52 (d, J = 3.3 Hz, 1H), 6.37 (dt, J = 0.6, 3.3 Hz, 1H), 5.24 (s, 2H), 4.54 (s, 2H), 2.65 (td, J = 1.2, 6.0 Hz, 2H), 2.54 – 2.44 (m, 2H), 1.85 – 1.65 (m, 4H).

**(5-(1-benzyl-1H-pyrazol-3-yl)furan-2-yl)methanol (57)**

LCMS: m/z (M + H)+ = 255.1.

**(5-(1-(pyridin-4-ylmethyl)-1H-indazol-3-yl)furan-2-yl)methanamine (58)**

LCMS: m/z (2M + H)+ = 609.4.

**(5-(1-(3-methoxybenzyl)-1H-indazol-3-yl)furan-2-yl)methanamine (59)**

LCMS: m/z (M + H)+ = 334.1, $^1$H NMR (400 MHz, $CD_3OD$) δ 8.13 (dt, J = 1.0, 8.2 Hz, 1H), 7.50 (dt, J = 1.0, 8.5 Hz, 1H), 7.40 (ddd, J = 1.1, 6.8, 8.5 Hz, 1H), 7.27 – 7.13 (m, 3H), 6.91 (d, J = 3.3 Hz, 1H), 6.82 – 6.73 (m, 2H), 6.44 (dt, J = 0.8, 3.4 Hz, 1H), 5.60 (s, 2H), 3.93 (s, 2H), 3.68 (s, 3H).

**(5-(1-(pyridin-2-ylmethyl)-1H-pyrazolo[4,3-b]pyridin-3-yl)furan-2-yl)methanol (60)**

LCMS: m/z (M + H)+ = 307.1, $^1$H NMR (400 MHz, $CD_3OD$) δ 8.61 (dd, J = 1.3, 4.4 Hz, 1H), 8.49 (ddd, J = 0.9, 1.8, 5.0 Hz, 1H), 8.09 (dd, J = 1.3, 8.6 Hz, 1H), 7.76 (td, J = 1.8, 7.7 Hz, 1H), 7.46 (dd, J = 4.4, 8.6 Hz, 1H), 7.31 (ddd, J = 1.1, 4.9, 7.7 Hz, 1H), 7.23 (d, J = 3.3 Hz, 1H), 7.17 (dt, J = 1.1, 7.8 Hz, 1H), 6.50 (d, J = 3.3 Hz, 1H), 5.78 (s, 2H), 4.63 (s, 2H).

**(5-(1-(pyridin-3-ylmethyl)-1H-pyrazolo[4,3-b]pyridin-3-yl)furan-2-yl)methanol (61)**

LCMS: m/z (M + H)+ = 307.1.

**(5-(1-(pyridin-4-ylmethyl)-1H-pyrazolo[4,3-b]pyridin-3-yl)furan-2-yl)methanol (62)**

LCMS: m/z (M + H)+ = 307.
**(5-(1-(pyridin-2-ylmethyl)-1H-pyrazolo[4,3-b]pyridin-3-yl)furan-2-yl)methanamine (63)**
Dimer in LCMS: m/z (2M)+ = 611.

**NCI Compounds**
**(4-(benzyl(ethyl)amino)-2-chlorophenyl)methanol (64)**
LCMS m/z (M + H+) 276.0
**(2-chloro-4-(ethyl(2-fluorobenzyl)amino)phenyl)methanol (65)**
LCMS: m/z (M + H)+ = 294
**(2-chloro-4-(ethyl(3-fluorobenzyl)amino)phenyl)methanol (66)**
LCMS: m/z (M + H)+ = 294
**(2-chloro-4-(ethyl(4-fluorobenzyl)amino)phenyl)methanol (67)**
LCMS: m/z (M + H)+ = 294.0
**(2-chloro-4-((2-chlorobenzyl)(ethyl)amino)phenyl)methanol (68)**
LCMS: m/z (M + H)+ = 310.0
**(2-chloro-4-((3-chlorobenzyl)(ethyl)amino)phenyl)methanol (69)**
LCMS: m/z (M + H)+ = 310.0
**(2-chloro-4-(ethyl(2-methylbenzyl)amino)phenyl)methanol (70)**
LCMS m/z (M + H+) 290.1
**(2-chloro-4-(ethyl(3-methylbenzyl)amino)phenyl)methanol (71)**
LCMS: m/z (M + H)+ = 290.1
**(2-chloro-4-(ethyl(4-methylbenzyl)amino)phenyl)methanol (72)**
LCMS m/z (M + H+) 290.1
**(2-chloro-4-(ethyl(2-methoxybenzyl)amino)phenyl)methanol (73)**
LCMS m/z (M + H+) 306.1
**(2-chloro-4-(ethyl(3-methoxybenzyl)amino)phenyl)methanol (74)**
LCMS m/z (M + H+) 306.1
**(2-chloro-4-(ethyl(4-methoxybenzyl)amino)phenyl)methanol (75)**
LCMS: m/z (M + H)+ = 306.1
**(2-chloro-4-((2,3-difluorobenzyl)(ethyl)amino)phenyl)methanol (76)**
LCMS: m/z (M + H)+ = 312

**(2-chloro-4-((2,4-difluorobenzyl)(ethyl)amino)phenyl)methanol (77)**
LCMS: m/z (M + H)+ = 312.0
**(2-chloro-4-((2,6-difluorobenzyl)(ethyl)amino)phenyl)methanol (78)**
LCMS: m/z (M + H)+ = 312.0
**(2-chloro-4-((3,5-difluorobenzyl)(ethyl)amino)phenyl)methanol (79)**
LCMS: m/z (M + H)+ = 312.0
**(2-chloro-4-((2-chloro-6-fluorobenzyl)(ethyl)amino)phenyl)methanol (80)**
LCMS: m/z (M + H)+ = 328
**(2-chloro-4-(ethyl(2-fluoro-6-methoxybenzyl)amino)phenyl)methanol (81)**
LCMS: m/z (M + H)+ = 324.0
**(2-chloro-4-(ethyl(2-fluoro-6-(trifluoromethyl)benzyl)amino)phenyl)methanol (82)**
LCMS: m/z (M + H)+ = 362
**(2-chloro-4-((2,6-dichlorobenzyl)(ethyl)amino)phenyl)methanol (83)**
LCMS: m/z (M + H)+ = 288.1

**(2-chloro-4-(ethyl(pyridin-2-ylmethyl)amino)phenyl)methanol (84)**
LCMS: m/z (M + H)+ = 277.0
**(2-chloro-4-(ethyl(pyridin-3-ylmethyl)amino)phenyl)methanol (85)**
LCMS: m/z (M + H)+ = 277.0
**(2-chloro-4-(ethyl(pyridin-4-ylmethyl)amino)phenyl)methanol (86)**
LCMS m/z (M + H+) 277
**(2-chloro-4-((4-fluorobenzyl)(methyl)amino)phenyl)methanol (87)**
LCMS m/z (M + H+) 280.0
**(2-chloro-4-((4-fluorobenzyl)(2-methoxyethyl)amino)phenyl)methanol (88)**
LCMS m/z (M + H+) 324.0
**(2-chloro-4-((cyclopropylmethyl)(4-fluorobenzyl)amino)phenyl)methanol (89)**
LCMS: m/z (M + H)+ = 320.0
**(2-chloro-4-(cyclobutyl(4-fluorobenzyl)amino)phenyl)methanol (90)**
LCMS: m/z (M + H)+ = 320.0
**(4-(bis(4-fluorobenzyl)amino)-2-chlorophenyl)methanol (91)**
LCMS: m/z (M + H)+ = 374.0
**(2-chloro-4-(8-fluoro-3,4-dihydroisoquinolin-2(1H)-yl)phenyl)methanol (92)**
LCMS: m/z (M + H)+ = 292.0
**(2-chloro-4-(1-methyl-3,4-dihydroisoquinolin-2(1H)-yl)phenyl)methanol (93)**
LCMS: m/z (M + H)+ = 288.1
**(2-chloro-4-(3,4-dihydroisoquinolin-2(1H)-yl)phenyl)methanol (94)**
LCMS: m/z (M + H)+ = 274
**(furan-2,5-diylbis(thiophene-5,2-diyl))dimethanol (95)**
LCMS: m/z (M + H)+ = 292.0
**4-(bis(2-chloroethyl)amino)-2-chlorobenzaldehyde (96)**
LCMS m/z (M + H+) 282

AUTHOR INFORMATION

Corresponding Author

Samarjit Patnaik email: samarjit.patnaik@nih.gov

Present Addresses

National Center for Advancing Translational Science, 9800 Medical Center Dr Rockville MD 20850. Phone 301.827.1772

ACKNOWLEDGMENT

This research was supported by the Molecular Libraries Initiative of the National Institutes of Health Roadmap for Medical Research Grant U54MH084681 and the Intramural Research Program of the National Center for Advancing Translational Sciences, National Institutes of Health.

## REFERENCES

(1) Valle, J.; Wasan, H.; Palmer, D. H.; Cunningham, D.; Anthoney, A.; Maraveyas, A.; Madhusudan, S.; Iveson, T.; Hughes, S.; Pereira, S. P.; et al. Cisplatin plus gemcitabine versus gemcitabine for biliary tract cancer. *N Engl J Med* **2010**, *362* (14), 1273-1281. DOI: 10.1056/NEJMoa0908721

(2) Shi, L.; Shen, W.; Davis, M. I.; Kong, K.; Vu, P.; Saha, S. K.; Adil, R.; Kreuzer, J.; Egan, R.; Lee, T. D.; et al. SULT1A1-dependent sulfonation of alkylators is a lineage-dependent vulnerability of liver cancers. *Nat Cancer* **2023**, *4* (3), 365-381. DOI: 10.1038/s43018-023-00523-0

(3) Ko, F. N.; Wu, C. C.; Kuo, S. C.; Lee, F. Y.; Teng, C. M. YC-1, a novel activator of platelet guanylate cyclase. *Blood* **1994**, *84* (12), 4226-4233. From NLM Medline.

(4) Friebe, A.; Koesling, D. Mechanism of YC-1-induced activation of soluble guanylyl cyclase. *Mol Pharmacol* **1998**, *53* (1), 123-127. DOI: 10.1124/mol.53.1.123

(5) Yeo, E. J.; Chun, Y. S.; Cho, Y. S.; Kim, J.; Lee, J. C.; Kim, M. S.; Park, J. W. YC-1: a potential anticancer drug targeting hypoxia-inducible factor 1. *J Natl Cancer Inst* **2003**, *95* (7), 516-525. DOI: 10.1093/jnci/95.7.516

(6) Chang, L. C.; Lin, H. Y.; Tsai, M. T.; Chou, R. H.; Lee, F. Y.; Teng, C. M.; Hsieh, M. T.; Hung, H. Y.; Huang, L. J.; Yu, Y. L.; et al. YC-1 inhibits proliferation of breast cancer cells by down-regulating EZH2 expression via activation of c-Cbl and ERK. *Br J Pharmacol* **2014**, *171* (17), 4010-4025. DOI: 10.1111/bph.12708

(7) An, H.; Kim, N. J.; Jung, J. W.; Jang, H.; Park, J. W.; Suh, Y. G. Design, synthesis and insight into the structure-activity relationship of 1,3-disubstituted indazoles as novel HIF-1 inhibitors. *Bioorg Med Chem Lett* **2011**, *21* (21), 6297-6300. DOI: 10.1016/j.bmcl.2011.08.120

(8) **D**evelopmental**T**herapeutic**P**rogram. *https://dtp.cancer.gov/databases_tools/data_search.htm*.

(9) Tools, N.-A. *https://discover.nci.nih.gov/cellminer/*.

(10) Huang, X.; Cao, M.; Wang, L.; Wu, S.; Liu, X.; Li, H.; Zhang, H.; Wang, R. Y.; Sun, X.; Wei, C.; et al. Expression of sulfotransferase SULT1A1 in cancer cells predicts susceptibility to the novel anticancer agent NSC-743380. *Oncotarget* **2015**, *6* (1), 345-354. DOI: 10.18632/oncotarget.2814

(11) Rothman, D. M.; Gao, X.; George, E.; Rasmusson, T.; Bhatia, D.; Alimov, I.; Wang, L.; Kamel, A.; Hatsis, P.; Feng, Y.; et al. Metabolic Enzyme Sulfotransferase 1A1 Is the Trigger for N-Benzyl Indole Carbinol Tumor Growth Suppression. *Chem Biol* **2015**, *22* (9), 1228-1237. DOI: 10.1016/j.chembiol.2015.06.025
(12) Rees, M. G.; Seashore-Ludlow, B.; Cheah, J. H.; Adams, D. J.; Price, E. V.; Gill, S.; Javaid, S.; Coletti, M. E.; Jones, V. L.; Bodycombe, N. E.; et al. Correlating chemical sensitivity and basal gene expression reveals mechanism of action. *Nat Chem Biol* **2016**, *12* (2), 109-116. DOI: 10.1038/nchembio.1986
(13) Meng, L. H.; Shankavaram, U.; Chen, C.; Agama, K.; Fu, H. Q.; Gonzalez, F. J.; Weinstein, J.; Pommier, Y. Activation of aminoflavone (NSC 686288) by a sulfotransferase is required for the antiproliferative effect of the drug and for induction of histone gamma-H2AX. *Cancer Res* **2006**, *66* (19), 9656-9664. DOI: 10.1158/0008-5472.CAN-06-0796
(14) Zhao, C. Y.; Szekely, L.; Bao, W.; Selivanova, G. Rescue of p53 function by small-molecule RITA in cervical carcinoma by blocking E6-mediated degradation. *Cancer Res* **2010**, *70* (8), 3372-3381. DOI: 10.1158/0008-5472.CAN-09-2787
(15) Celegato, M.; Messa, L.; Goracci, L.; Mercorelli, B.; Bertagnin, C.; Spyrakis, F.; Suarez, I.; Cousido-Siah, A.; Trave, G.; Banks, L.; et al. A novel small-molecule inhibitor of the human papillomavirus E6-p53 interaction that reactivates p53 function and blocks cancer cells growth. *Cancer Lett* **2020**, *470*, 115-125. DOI: 10.1016/j.canlet.2019.10.046
(16) Singh, M.; Zhou, X.; Chen, X.; Santos, G. S.; Peuget, S.; Cheng, Q.; Rihani, A.; Arner, E. S. J.; Hartman, J.; Selivanova, G. Identification and targeting of selective vulnerability rendered by tamoxifen resistance. *Breast Cancer Res* **2020**, *22* (1), 80. DOI: 10.1186/s13058-020-01315-5
(17) Frame, L. T.; Ozawa, S.; Nowell, S. A.; Chou, H. C.; DeLongchamp, R. R.; Doerge, D. R.; Lang, N. P.; Kadlubar, F. F. A simple colorimetric assay for phenotyping the major human thermostable phenol sulfotransferase (SULT1A1) using platelet cytosols. *Drug Metab Dispos* **2000**, *28* (9), 1063-1068.
(18) Mulder, G. J.; Hinson, J. A.; Gillette, J. R. Generation of reactive metabolites of N-hydroxy-phenacetin by glucoronidation and sulfation. *Biochem Pharmacol* **1977**, *26* (3), 189-196. DOI: 10.1016/0006-2952(77)90301-x.
(19) Avdeef, A.; Bendels, S.; Tsinman, O.; Tsinman, K.; Kansy, M. Solubility-excipient classification gradient maps. *Pharm Res* **2007**, *24* (3), 530-545. DOI: 10.1007/s11095-006-9169-0.
(20) Sun, H.; Shah, P.; Nguyen, K.; Yu, K. R.; Kerns, E.; Kabir, M.; Wang, Y.; Xu, X. Predictive models of aqueous solubility of organic compounds built on A large dataset of high integrity. *Bioorg Med Chem* **2019**, *27* (14), 3110-3114. DOI: 10.1016/j.bmc.2019.05.037.
(21) Shah, P.; Kerns, E.; Nguyen, D. T.; Obach, R. S.; Wang, A. Q.; Zakharov, A.; McKew, J.; Simeonov, A.; Hop, C. E.; Xu, X. An Automated High-Throughput Metabolic Stability Assay Using an Integrated High-Resolution Accurate Mass Method and Automated Data Analysis Software. *Drug Metab Dispos* **2016**, *44* (10), 1653-1661. DOI: 10.1124/dmd.116.072017.
(22) Di, L.; Kerns, E. H.; Gao, N.; Li, S. Q.; Huang, Y.; Bourassa, J. L.; Huryn, D. M. Experimental design on single-time-point high-throughput microsomal stability assay. *J Pharm Sci* **2004**, *93* (6), 1537-1544. DOI: 10.1002/jps.20076.
(23) Sun, H.; Nguyen, K.; Kerns, E.; Yan, Z.; Yu, K. R.; Shah, P.; Jadhav, A.; Xu, X. Highly predictive and interpretable models for PAMPA permeability. *Bioorg Med Chem* **2017**, *25* (3), 1266-1276. DOI: 10.1016/j.bmc.2016.12.049.